Modeling of a grand piano action mechanism

Harmen Links

Master of Science Thesis

TU Delft Delft University of Technology

Delft Center for Systems and Control

Modeling of a grand piano action mechanism

Master of Science Thesis

For the degree of Master of Science in Systems and Control at Delft University of Technology

Harmen Links

April 1, 2011

Faculty of Mechanical, Maritime and Materials Engineering (3mE) · Delft University of Technology

Abstract

The piano action mechanism is a complex mechanism that makes up an important part of the construction of modern grand pianos. Its design is a key factor in the quality of a grand piano as it involves both tone and touch of the instrument. Even though there has been quite some gain in technological knowledge in general in the past century, the design of the action mechanism has not changed much over this period and even the used materials are quite unchanged. This is not only caused by the conservatism of the building industry but more so by the fact that the design has proven to be very functional. The action mechanism consists of mainly wooden parts, and to prevent noises during operation the contacts between these parts are overlaid with felt and leather materials. The main function of the mechanism is to work as a lever that accelerates the hammer to a velocity that is many times the key velocity when the key is struck by a pianist. Next to this, it also provides the possibility of fast repetition of notes by a smart construction of intermediate levers. During operation, the mechanism exhibits different stages of movement where the configuration changes and parts make and break contact.

This project was initiated by the idea to develop a simulation-tool that can be used by piano technicians when regulating or restoring an instrument. Piano technicians regulate and prepare the action mechanism according to partly standard rules given by the manufacturer and partly experience and unverified assumptions. A dynamical simulation that gives insight in the physics behind the workings of the action mechanism and its effect on tone and touch can be used by a piano technician to make a founded judgement on possible improvements that can be made through regulation or replacing parts of the action mechanism.

To develop such a simulation-tool, the first goal of this project was to build a dynamical model of the action mechanism that captures the important dynamical and configuration properties of a real life mechanism. This includes the regulation settings that can be adjusted by a technician to change the configuration, but also material properties that change when parts are replaced. In order to build a model with these properties, a multi body modeling method is used where the action mechanism is represented as five rigid bodies with contact dynamics. The dynamical equations were derived using Lagrange's equations with explicit holonomic constraints provided with Lagrange multipliers for hard contact and custom made force equations for contact with elasticity and damping. The principle of a hybrid automata

is used to switch between subsets of the constraints during operation of the mechanism. To provide a realistic interaction between the action mechanism and the strings in a grand piano and to relate the output of the action model to the sound of the instrument, also a dynamical string model is developed. For this a 1D wave equation for transverse vibrations is extended with stiffness and damping terms and discretized in the space variable to form a state space model. This string model is coupled with the model of the action mechanism to make parallel simulation possible.

Comparison of the simulated output of the model to measurements that were extracted from high speed video images showed an agreement for different intensities of keystrokes. Also different types of keystrokes can be simulated, that is a pressed keystroke where the hammer is held in the repetition position after hitting the string and a struck type of keystroke where the hammer bounces back to its initial position. The simulated string vibrations shows that the excited harmonic frequencies and there magnitude correspond to measured sound for keystrokes with different intensity, that is for a range of different input signals. The simulation is analyzed in terms of accuracy and usability for a practical problem and possible improvements are pointed out. Also interesting subjects for further study are given in the concluding chapter.

Table of Contents

Preface

This document is a part of my graduation project for the Master of Science program in Systems & Control at Delft University of Technology. My interest for the subject of this report came after a discussion with my piano tuner Mr. W.Vreeken about the high demands that some pianists have on the performance of their instruments, and the limited possibilities of a piano tuner to regulate and prepare the instrument. The idea of doing my final project on the subject came a bit later when I discussed my thought of modeling the piano mechanism with Dr. A.J.J. van den Boom and Prof. D.J. Rixen. They gave me the possibility to bring my idea into practice.

To facilitate my project, several people played a crucial role and I would like to thank them for there efforts. First, I would like to thank my supervisor Dr. A.J.J. van den Boom for the regular discussions we had about my project work and his critical review of my reports. Also I would like to thank Prof. D.J. Rixen for his occasionally guidance and comments on my memos that were always on a stimulant tone. I would like to thank Dr. A. Schwab for telling me what I needed to know about multi body dynamics and for his critical view on my draft report. To build the lab setup that I needed to do some experiments on, with my budget of 0 Euros, I was greatly helped by Mr. W.Vreeken who helped me to select the needed materials and gave me instructions. Also Mr. J. van Driel helped me a lot with selecting the sensors and data acquisition material for my lab setup and he provided me with a working space at the measurement shop.

Last but not least, I would also like to thank my brother, who let me stay at his house for the past 9 months, it was a pleasant stay.

Delft, University of Technology — Harmen Links
April 1, 2011

Chapter 1

Introduction

1-1 Motivation

The technical quality of a grand piano can be measured by two characteristics. The first is the sound produced by the instrument which is called the tone and the second is the haptic response the pianist experiences when playing which is called the touch of the instrument. The action mechanism is the one part of the grand piano influences both characteristics, hereby it can be said that the action mechanism is a crucial part in the design of the modern grand piano.

The initiation of this project started with the idea to develop a simulation-tool that can be used by a piano technician when regulating or restoring an instrument. Piano technicians regulate and prepare the action mechanism according to partly standard rules given by the manufacturer and partly experience and unverified assumptions. A dynamical simulation that can give insight in the physics behind the workings of the action mechanism and its effect on tone and touch can be used by a piano technician to make a founded judgment on possible improvements that can be made trough regulation or replacing parts of the action mechanism.

The first goal of this project is to develop a dynamical model of the action mechanism with parameters for configuration and dynamical properties. And to be able to relate the output of this model to the tone, also a dynamical string model will be developed. It is aimed for that with such a simulation, the effect of changing regulation settings and material properties on the motion of the mechanism and the produced tone can be predicted.

1-2 Construction of the grand piano

Modern grand pianos come in different sizes and quality but they all share the same construction. Figure 1.1 shows a one-key setup of an action mechanism with a tri chord string for the tone C5 on a grand piano. This can be seen as a cross-cut of the instrument where the soundboard is left out.

Figure 1-1: one key setup of the action mechanism

A modern grand piano has 88 keys with 250 corresponding strings of which the mid and higher ranges are duo and tri chord unisons tightened in a cast iron frame. This frame supports a tension ranging from 100N to 500N per string giving a total of approximately 75 kN of tension force. The string tension is adjustable with the tuning pins mounted in a wooden pinblock. The strings are guided via the agraffes over the bridge and rigidly connected to the cast iron frame. This shows that the speaking length of the string (first mode of free vibration) is the length between the agraffe and the bridge. This bridge transfers the mechanical vibrations of the strings to the sound board which amplifies the vibrations causing pressure waves in the air in the vicinity of the soundboard. These pressure waves are audible sounds in the range of A0 to C8 which theoretically corresponds to fundamental frequencies of 27.8 Hz to 4186.01 Hz for an equal temperament tuning scheme [18]. The 88 keys of a modern grand piano are connected to the action mechanism with about 65 unique parts per key.

1-3 History of the grand piano

One could say the action mechanism is the one part distinguishing the piano from its ancestor, the harpsichord. Therefore the history of the development of the action mechanism is also the majority of adjustments made to the design of the total instrument. In 1709 the Italian harpsichord maker Bartolomeo Cristofori replaced the plectrums in a harpsichord by small leather hammers to strike the strings. This new concept asked for several adjustments of the action mechanism, which he made in the subsequent years. A final version of Cristoforis mechanism dating from 1726 already showed the major properties of the action mechanism used in modern grand pianos. The hammerhead was placed on a shank resting on an intermediate lever close to its pivoting point, this construction transfers the motion of the key such that the hammer lifts of with a velocity which is many times the key velocity. Although the main features of this action were already quite similar to the modern action design there were two big adjustments to be made in the nineteenth century.

The French piano builder Erard invented the double repetition action in 1821, which makes it possible to play faster repetitions as the name does expect. This repetition function can be found in the construction of the whippen assembly as used in a modern action mechanism. Erard was also the first to put pedals on the piano. A few years later in 1826 an also French piano technician named Pape tried felt hammers instead of the leather ones. As small as this adjustment may seem this invention heavily contributed to the characteristic tone and dynamic range of the piano as we know it today. After these adjustments the action

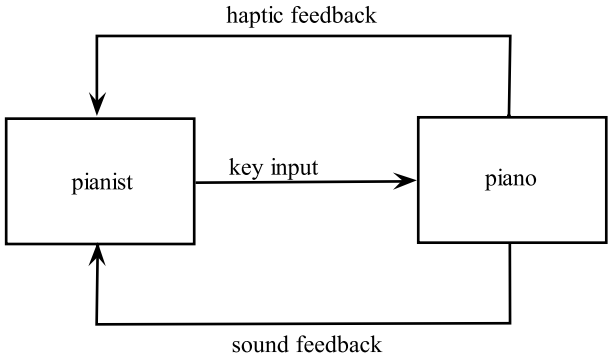

Figure 1-2: the grand piano as a system that interacts with the pianist

mechanism was refined some more in the course of the nineteenth century but no major things were changed in the construction ref. [4] and [17].

1-4 Systems and signals

When the instrument is played, the musician processes the feedback of sound and haptic touch and responds by adjusting the key input. This is indicated with the block diagram in figure 1-2. The processing of the feedback of sound involves musicality, artistic impression and the interpretation of sound, which are all very complex psychological aspects. In spite of this, the sound of the instrument can be described by two physical characteristics from which it is known how they influence the human perception, namely the frequency content and the magnitude of the relative sound pressure. The musician can adjust the key input to create a tone within the dynamical range and timbre of the instrument. A very soft key input results in a tone with relative small magnitude and just a few harmonic frequencies which is referred to as pianissimo playing, while a very hard key input results in a tone with relative large magnitude and more harmonic frequencies, this is referred to as fortissimo playing. Next to the processing of the feedback of sound the processing of the haptic feedback can also be regarded as a psychological matter. The haptic feedback can be characterized by the relation between the force that is exerted on the key and the resulting velocity change of the surface where the pianists finger is in contact with the key. This is strongly related to the feeling of control that a pianist experiences when playing the instrument. As this description of figure 1-2 may give the impression that the pianist makes only instantaneous decisions on how to strike the keys it must be mentioned that a skilled pianist has had several years of training and uses his or her motorial memory exhaustively.

To analyze the physics of a grand piano it is common approach to divide the instrument in three mechanical systems as action mechanism, strings and soundboard together forming a series connection as shown in figure 1-3. There is a two way interaction between these systems indicated with the arrows in both directions. The key input of a pianist is the input of the action mechanism which can be characterized as a force Fk that varies over time. This force results in a key velocity vk. The relation vk/Fk is referred to as mechanical admittance and

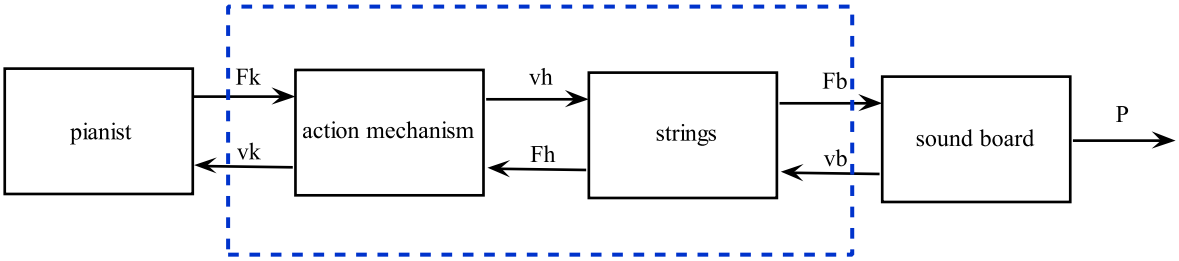

Figure 1-3: grand piano as a series of mechanical systems with the boundary of this project

is a measure for the haptic touch that a pianist experiences ref. [4]. The action mechanism uses this input force to accelerate the hammer which causes the hammer to lift off with a velocity vh to impact the string. The interaction with the string exerts a reaction force Fh on the hammer and causes it to bounce back. The impact of the hammer on the string excites several resonance modes of the string and these vibrations are transfered via a bridge to the sound board. That is, the vibrations exert a force Fb on the bridge that causes a displacement with velocity vb and this causes the soundboard to vibrate. The vibrations of the soundboard cause air pressure waves P in the vicinity of the instrument, that we experience as the tone of a grand piano.

1-5 Literature survey

A lot of researchers have spend there time investigating the physics of musical instruments in the past century. It can be noticed that most of this research had an experimental character and the results where mostly for academic purpose. A highly noticeable fact is that at the time that the scientific research started, most instruments where already developed to the modern instruments we know today. Hence, it can be concluded that the design of the majority of modern acoustical musical instruments is optimized by adjustments based on trial and error and feedback from musicians. This also holds for the grand piano as explained briefly in chapter 1-3. When we focus on the action mechanism and strings of a grand piano, there is just a select group of research. However, the motivations for this research vary from the gain of theoretical knowledge for academic purpose to investigating the possibility of building electronic keyboards that mimic the haptic touch of a real piano.

One of the first research in the physics of the action mechanism was done by P.R.Dijksterhuis [1] who published an article in 1965 that describes some experiments on the interaction between the key and hammer of a mechanism and uses this to derive some simple equations of motion. He showed that the action mechanism can be viewed on as a mechanical system that translates a mechanical impulse into a final hammer velocity and it is hereby possible to produce the same tone with seemingly different keystrokes. Dijksterhuis relates his results to studies of rhythmical aspects of piano performance. One of his conclusions was that the touch of the pianist has no direct influence on the tone of the instrument. This statement was received with a lot of criticism in the musical world. More recent studies concerning the timing of the action mechanism is given by Askenfelt and Jansson [2] and Goebl, Bresin and

Galembo [11]. They describe the timing properties of the mechanism very detailed. Some of the most extensive research on modeling the action mechanism is done by B.Gillespie who worked on a PhD project from 1992 to 1996 [3,4].The research of Gillespie was motivated by the desire to develop electronic keyboards that feel, respond and sound like real pianos. It was aimed for to develop a dynamical model which describes the haptic touch of a real action mechanism and to use this model to control some actuators attached to the keys of an electronic key-board to simulate such a response. He used a multi body modeling approach with kane's method to derive the dynamical equations. This resulted in a very extensive set of ODEs that covered every possible configuration of the mechanism during operation. The Japanese researchers Hayashi, M.Yamane & H. Mori successfully used a dynamical model of the action mechanism to built a computer controlled piano [10]. This resulted in one of the first automatic playing pianos that used the full dynamical range of the instrument. The controller they designed was based on a frequency domain model that they gained from experiments. The most recent effort in modeling the action mechanism is done at the Waterloo university under guidance of Stephen Birkett and John McPhee in the period of 2003 to 2009 ref. [5] to [8]. This research is funded by Steinway pianos and several students worked on the project. They developed a dynamical model based on linear graph theory with specialized modeling software for the Maple computing environment. With this modeling software they had the possibility to include contact dynamics with custom made equations that they derived from experiments. The model was later on extended with a dynamical string model and a flexible body for the hammer, to simulate a realistic contact between hammer and string. They showed with simulations that the scuffing motion between hammer and string that occurs with flexible hammer shafts, can have a little influence on the tone. The string model they used was based on a 1D wave equation for transverse vibrations with additional stiffness term and they solved this equation using mode superposition. More extensive string models are presented in the PhD thesis of Balázs Bank [26] on physics-based sound synthesis of string instruments. The research of Bank was motivated by the idea to develop algorithms to implement in a digital synthesizer to create a realistic piano tone. He presents several strategies to model both transverse and longitudinal vibrations in strings including damping and nonlinear effects. The interaction between hammer and string has more often been the subject of research, probably because the dynamics of the hammer felt is known to have a big influence on the tone. One of the first to describe the nonlinear dynamics of hammer felt and the effect on the interaction with the strings was D. E. Hall [16].

Chapter 2

Investigating the action mechanism

2-1 Configuration and workings

In figure 2-1 a picture of a one key setup of the mechanism is given with names for the most important parts. The regulation parts are left out as this will be discussed in paragraph 2-3 and for convenience the less important parts are also left out because this amounts up to over 50 unique parts for a one key configuration.

From the perspective of tone production, the function of the action mechanism is twofold. First, the action mechanism has to function as a lever with a ratio of about 1:5 and second, with the smart construction of intermediate levers a repetition function is provided. To make a functional description of the workings of the mechanism, it suffices to distinguish between four motion stages. In chapter three a technical description of the workings will be set up where it turns out that there is need for more then ten stages to describe all events during operation. For now, as already mentioned a description with four stages is sufficient, this is also in line with descriptions in [2] and [4].

Figures 2-2 to 2-5 show the configuration of the mechanism for each of the four stages with the five most important parts, the key in green, the whippen in red, the bridge in purple , the jack in yellow and the hammer in orange. The parts of the mechanism are cut with blue lines when they are in motion relative to the stationary frame and with black lines when they are in rest. red-yellow circles are placed on the rotational joints when they are active.

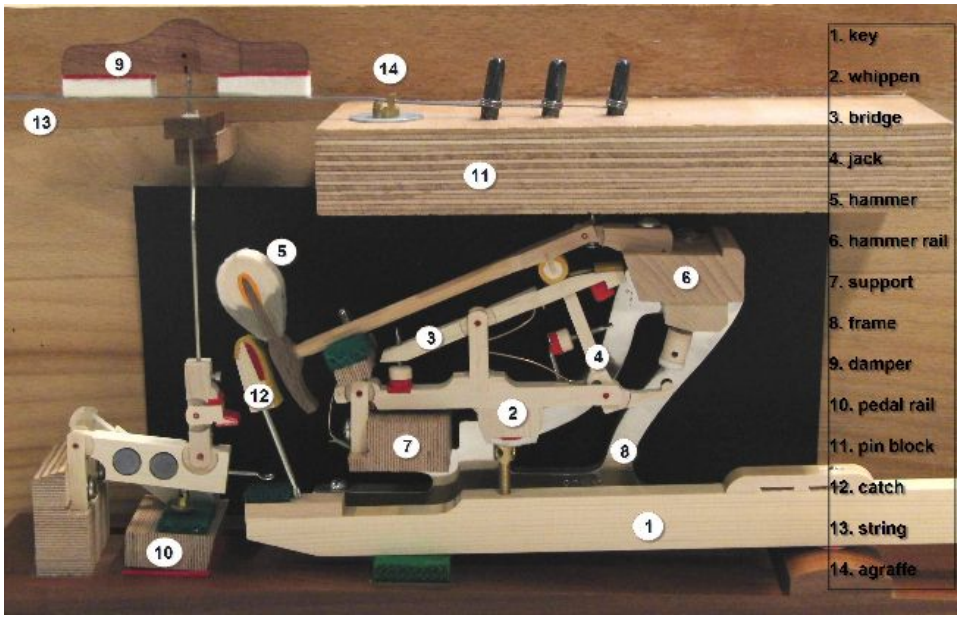

Figure 2-1: one key configuration of the mechanism with names of the most important parts

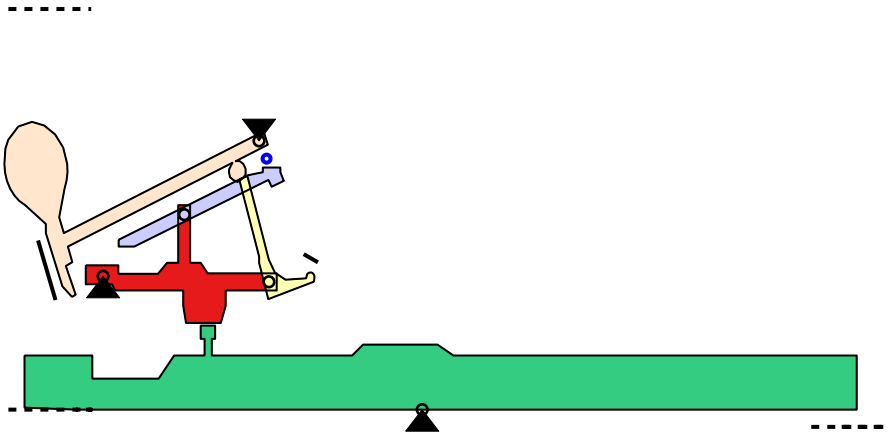

Figure 2-2: *I Rest*: All parts are in their rest position.

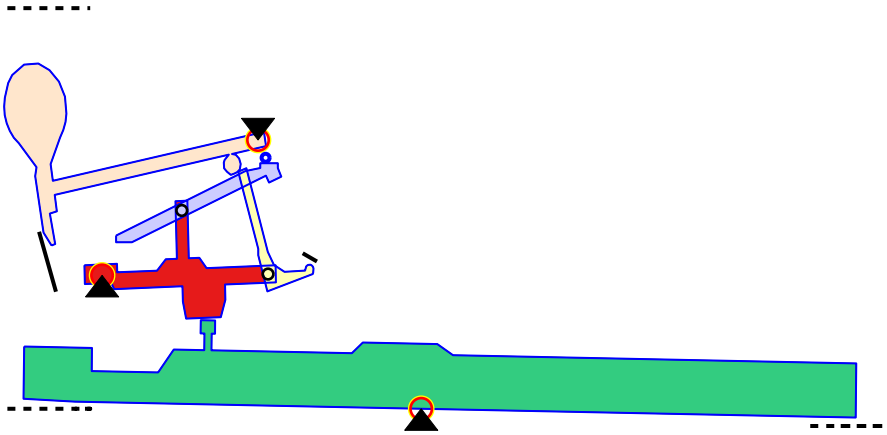

Figure 2-3: *II Acceleration*: When a key stroke is applied to the key, the whippen assembly, consisting of whippen, bridge and jack moves up as if it was one part. The purpose of this stage is to accelerate the hammer.

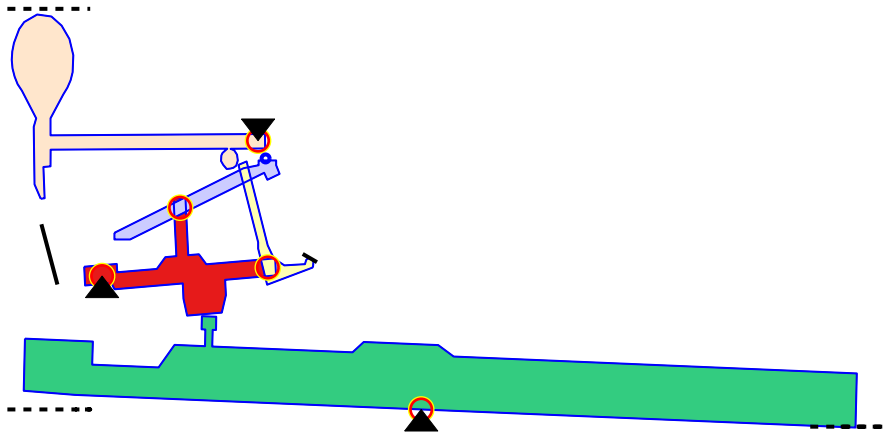

Figure 2-4: *III Let off* : The let off is initiated when the jack-toe hits the set off button, this causes the jack to rotate from under the hammer-knuckle and the hammer lifts of with a constant velocity to hit the string. Also the bridge hits the drop screw to rest in its repetition position and the key hits the key bed.

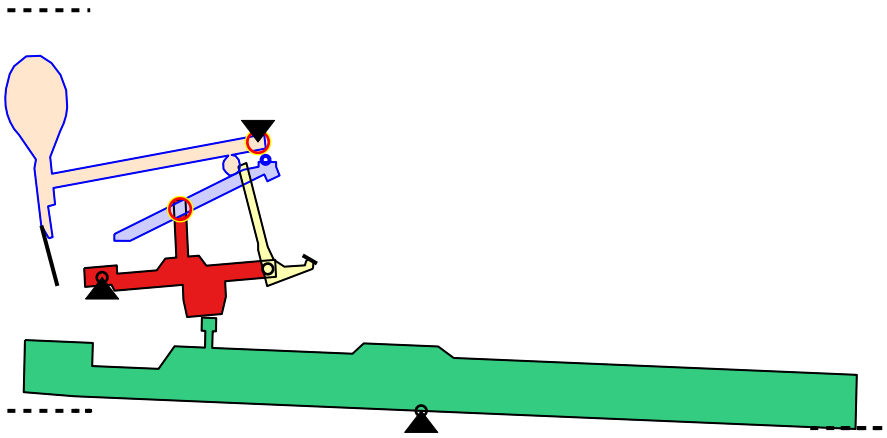

Figure 2-5: *IV Catch* : The hammer is bounced back by the string and the knuckle lands on the bridge. It remains in this position while the key is pressed. From this configuration there are two possibilities, either the key is released and the mechanism goes back to rest (I) or the key is struck again after the jack turned back under the knuckle.

2-2 Haptics

The word haptics is used to refer to the perceptual sense of touch which includes both senses of skin and muscles. This is a subject that is treated by research that ranges from robotics to biology. For the piano and probably also other musical instruments, haptics is referred to as touch of the instrument.

As seen from the perspective of touch, the function of the action mechanism is to serve as an interface between the pianist and the sound producing parts of a grand piano. Here the feeling of control that the pianist experiences is essential, which is fairly difficult to specify in technical terms. However, there are some attempts described in literature [4]. A few points of interest found in literature are given in the table below.

	smallest observable change
Sensing tactile force static	0.25 N
Sensing tactile force dynamical	0.5 N
Spinal reflex	40 ms
Conscious reflex	150 ms

When a grand piano is newly build it is aimed for to even out the down weight of the keys so that the static force that is needed to push down the keys is equal over the whole keyboard. This method is known as static balancing according to ref. [25]. Because the weight of the hammers varies quite a lot over the range of the keyboard, this method is not sufficient from a dynamical point of view. The force resistance felt at the key due to the rotational inertia

of the hammer is not influenced by evening out the down weight of the keys, and as a result a pianist can experience a very uneven feel over the range of the keyboard when only static balancing is applied.

2-3 Regulating the action

Several adjustments can be made by a piano technician in order to regulate and prepare an action mechanism. The most important ones are numbered in figure 2-6 and will be explained in the following text. Regulating an action mechanism can be depicted as a standard procedure where a road map is followed step by step, such a road map is given in the appendix . This most often leads to fulfilling results, however when a mechanism has to be tuned to meet the preferences of a pianist, conflicting specifications arise. When a grand piano is regulated before a concert when very soft playing is preferred, adjustments can be made so that the distance that the key is in direct contact with the hammer is maximal, which provides a feeling of control to the pianist. A drawback of such an adjustment is that the keys have to be pressed down all the way to accelerate the hammer and this can be experienced as if the dynamical range of volume of the tone is narrowed. It can also be a limitation for fast playing. Next to the standard regulation, adjusting the weight of hammer and key is used to change touch and tone. A noticeable fact is that the force resistance felt at the key due to the rotational inertia of the hammer is quadratically proportional to the leverage ratio, which indicates that these effects can be reduced by adjusting the leverage ratio of the mechanism.

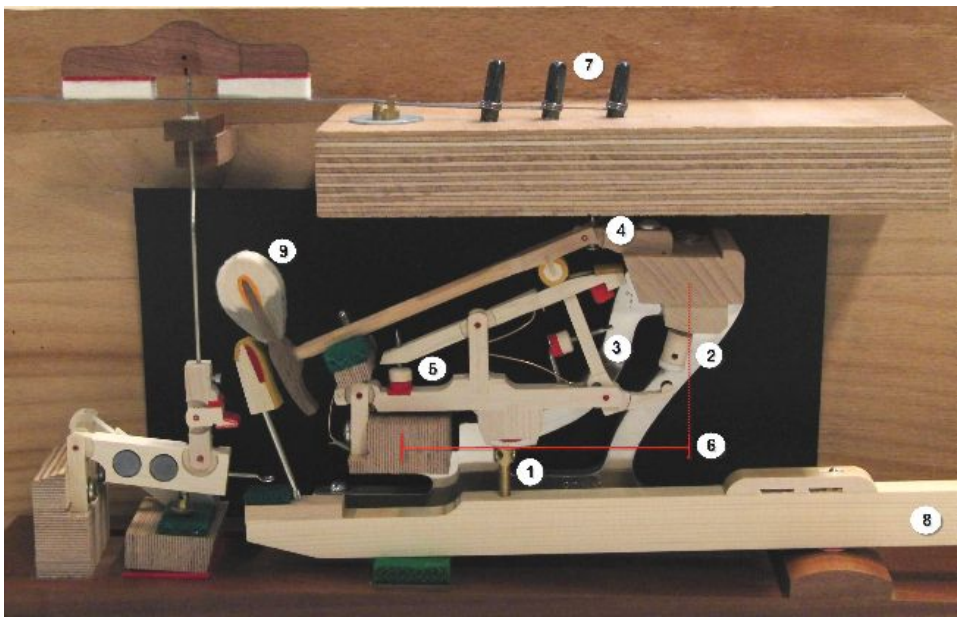

Figure 2-6: one key configuration of the mechanism with locations of regulation adjustment points

1. *Capstan*: The capstan is a metal screw that is mounted on the key to support the whippen assembly. Its hight can be adjusted to set the hammer travel distance.
2. *Set off button*: This button can be adjusted to change the hammer let off moment, that is initiated by the jack hitting the set off button.
3. *Jack regulator screw*: With this screw the angle that the jack makes with the whippen can be adjusted.
4. *Drop screw*: This screw determines the hight where the bridge stops in its repetition position.
5. *Bridge regulating screw*: This screw sets the initial hight for the bridge.
6. *Support-hammer rail distance*: This is the distance between the wooden rail where the hammers are mounted on and the rail that supports the whippen assembly. This distance can be varied a little be adjusting the whippen support rail.
7. *Tuning pins*: When the pins are rotated the tension in the strings varies. The tuning pins are used to tune the piano.
8. *Key leads*: Little lead rolls can be placed inside the key to statically balance the key board.
9. *Hammer head*: Hammer heads can be replaced and also little leads can be added or material can be removed to adjust its weight.

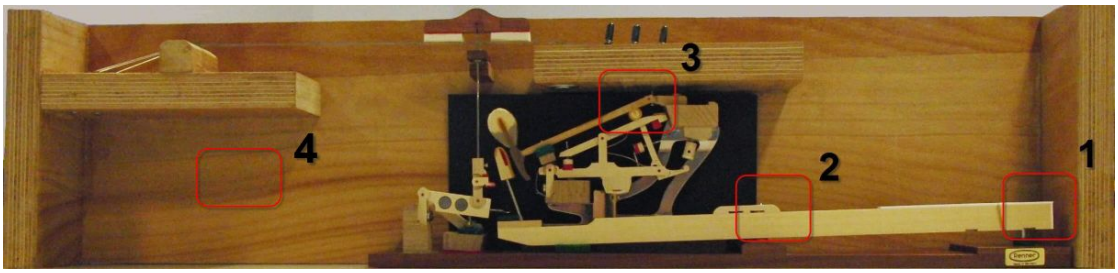

Figure 2-7: lab setup with sensor locations

2-4 Setup and sensors

To be able to do some experiments and tests on a real life mechanism, a one-key lab setup was built. For this the parts of a Renner mechanism were used. This type of mechanism is used in various brands of modern grand pianos. Also a casing was built to support a set of strings that correspond to a C5 tone on a grand piano and the hammer of the mechanism was replaced to match this tone. A picture of the lab setup is given in figure 2-7 with the locations of the sensors.

As explained in chapter 1-4, the mechanism can be viewed on as a mechanical system that translates a force profile to a constant final hammer velocity. So these two signals are of biggest interest. However, to be able to identify different events during operation of the mechanism also the motion of intermediate levers is of interest. To measure the force at the key, a piezo-film sensor was placed on the key at position 1. This type of sensor is chosen because it adds just a little bit of weight < 0.5 grams to the key which is less then 1% of the total weight of the key and the cost-price is very low. Furthermore a laser position sensor was used to measure the key displacement at position 2. As there is not enough space between the pin block and hammer shaft on the lab setup to mount a laser displacement sensor at position 3, another method had to be used to measure the hammer displacement. For this, a high speed video camera was used and to extract motion profiles from the video data a little software tool was developed using OpenCV. With this technique also the motion of the intermediate levers can be measured. At position four a microphone is positioned to record the sound the is produced by the vibrating string. Noticeably, the sound of the lab setup closely resembles the sound of a real piano with the only difference being the presence of a soundboard.

2-5 High speed video data

A Phantom High speed digital video camera was used to make video recordings of the motion of the mechanism during operation. This video camera is capable of recording at a sample frequency of 1kHz with a full resolution of 1024x1024 pixels. This is fast enough to record all events during operation of the mechanism, however it is not sufficiently fast to capture string vibrations as the ground frequency of the string is about 500 Hz.

To extract the motion data from the videos, a little software tool was made to track the motion of objects in a video. For this the OpenCV C++ library was used. OpenCV is an

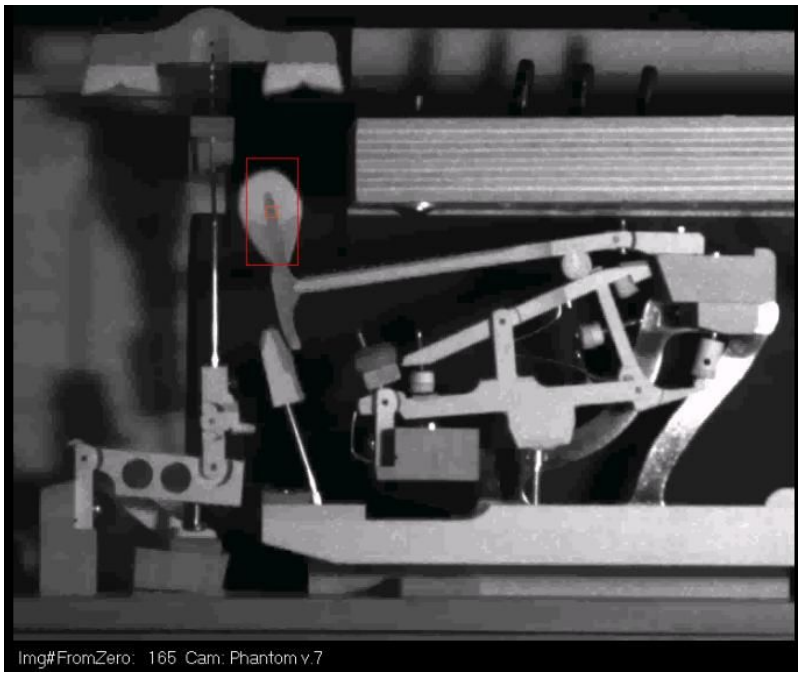

Figure 2-8: screen shot of video with mean-shift tracking window on the hammer head

open source computer vision library that originated in 1999 with the cooperation of Intel and 2006 a first official version was released. The library is supported with a book [13] to learn to how to use it.

For the motion tracking, the mean-shift algorithm is used. The mean-shift algorithm is a mathematical method to find local maxima in some distribution of a data set [12]. In the OpenCV library, the algorithm is implemented in the function cvMeanShift() to be used for object tracking in video data. This function allows the user to choose a feature distribution in a video frame that represents the object that is to be tracked in the next video frame. This feature distribution can be based on color and texture, but also intensity or gray values can be used. As the videos from the Phantom camera are recorded with gray values, a histogram of gray values within a selected window is used as a feature distribution for the mean-shift algorithm. In figure 2-8 a screen shot is given where the object tracking is in action, the hammer head is selected as an initial feature distribution shown as the red window with fixed size and this way the motion of the hammer head is tracked frame by frame.

2-6 Measurements and observations

To analyze the action mechanism a few experiments are done where different key strokes are applied and simultaneously different signals are recorded. The force at the key with the piezoelectric sensor, the displacement of the key with the laser sensor, the motion of the rest

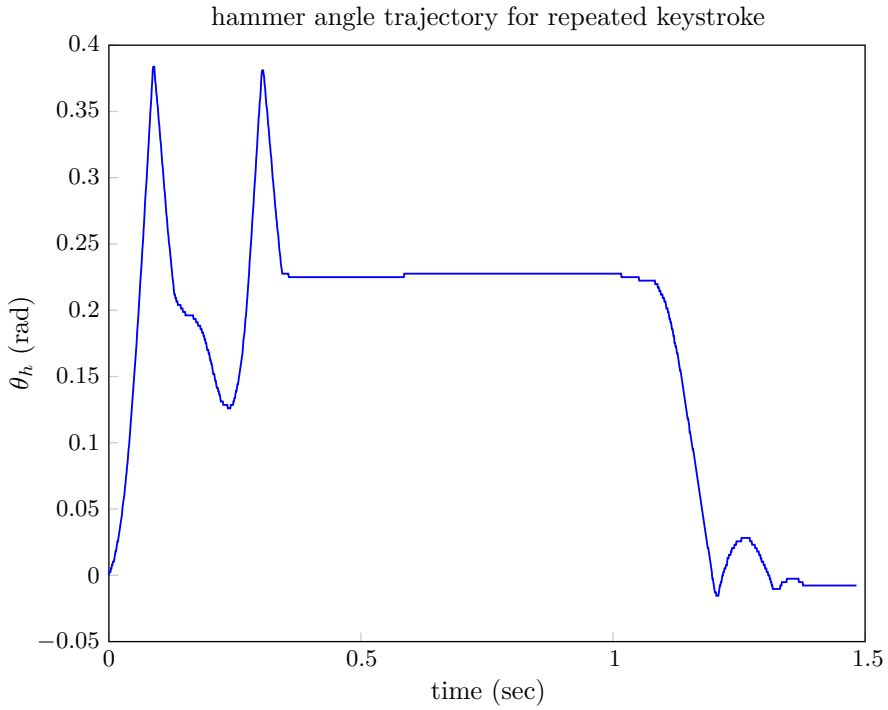

Figure 2-9: measurement of hammer trajectory for repeated keystroke extracted from video

of the mechanism with the high speed digital camera and the sound produced by the string vibrations with a microphone.

The first subject to investigate was the dynamical range of hammer trajectories. That is, the response of the mechanism to a range of different keystrokes. In figure 2-10 the measured force profiles at the key-tip are given for four pressed key strokes ranging from soft to very hard. In figure 2-11 the corresponding hammer trajectories are given. To characterize the keystrokes a difference can be made between a pressed legato and struck staccato type of touch. The forces in figure 2-10 are for pressed keystrokes with intensities soft, medium, hard and very hard corresponding to piano, mezzo-forte, forte and fortissimo playing respectively. The forces are plotted only for the time that they effectively contribute to the hammer movement, which is until the hammer lift-off. And the peak forces range from 0.5N for soft to 30N for a very hard keystroke. From the given hammer trajectories in figure 2-11 the different motion stages as described in chapter 2-1 can be distinguished. First the hammer is accelerated (II) then it hits the string (III) and bounces back to land on the catch and bridge/repetition lever (IV), at this point in time the key was still pressed down and thus the hammer stays in this position. The effect of the keystrokes with different intensities on the hammer trajectories is clearly visible in figure 2-11. As expected, the hammer traveling times range from approximately 220 ms for soft to 40 ms for a very hard keystroke. This indicates that the hammer reaches a higher velocity for higher intensities of the keystroke resulting in a higher impact force on the string. This also explains that after hitting the string, the time it takes to fall back on the catch and bridge is longer for the soft then for the hard keystroke.

	min	max
Key travel time	30ms	200ms
Hammer travel time	40 ms	220ms
Hammer free travel time	1ms	20ms
Hammer string contact time	1.5ms (ff)	4ms (pp)

Next to the key force and hammer angle trajectory also the frequency spectrum of the recorded sound is shown in figure 2-12 to 2-15 for the different keystrokes. For this a centered FFT is computed and normalized for the very hard keystroke data. The figures show that for keystrokes with higher intensity more harmonic overtones are present. These overtones correspond to vibration modes of the set of strings that are excited by the impact of the hammer. The first vibration mode of the set of strings that is used for the setup corresponds to about 523 Hz. For the soft keystroke only the first 6 modes have a significant contribution to the sound, for the medium keystroke also the 7th and 8th mode are excited a little, for the hard keystroke the 9th to 12th mode are also present and for the very hard keystroke the FFT shows that up to approximately the 30th mode of the set of strings is present in the sound.

These FFT signals in figure 2-12 to 2-15 thus show that for notes played with higher intensity, more harmonic overtones are excited. It can also be noticed that the slope of the decay of the frequency components is different for keystroke with different intensity. When we look at the slope over 6 octaves, that is 6 harmonic modes, for the soft keystroke the slope is app. -40 dB/6oct, for the medium keystroke app. -25dB/6oct and for the hard and very hard keystroke app -20 dB/6oct this is also mentioned in ref [26]. Also in figure 2-12 and 2-13 there is a significantly smaller contribution of the 9th mode, this corresponds to the position where the hammer hits the string according to ref [1] and [2]. In most pianos the impact position of the hammer is at a ratio of the length of the string somewhere between 1/7 and 1/10 such that the vibration mode that corresponds to this length is excited significantly less. In [17] and [26] the concept of phantom partials is treated, these overtones are not harmonic and are caused by longitudinal vibrations in the string and flexible string boundary. Noticeably, such enharmonic overtones are not present in the measurement.

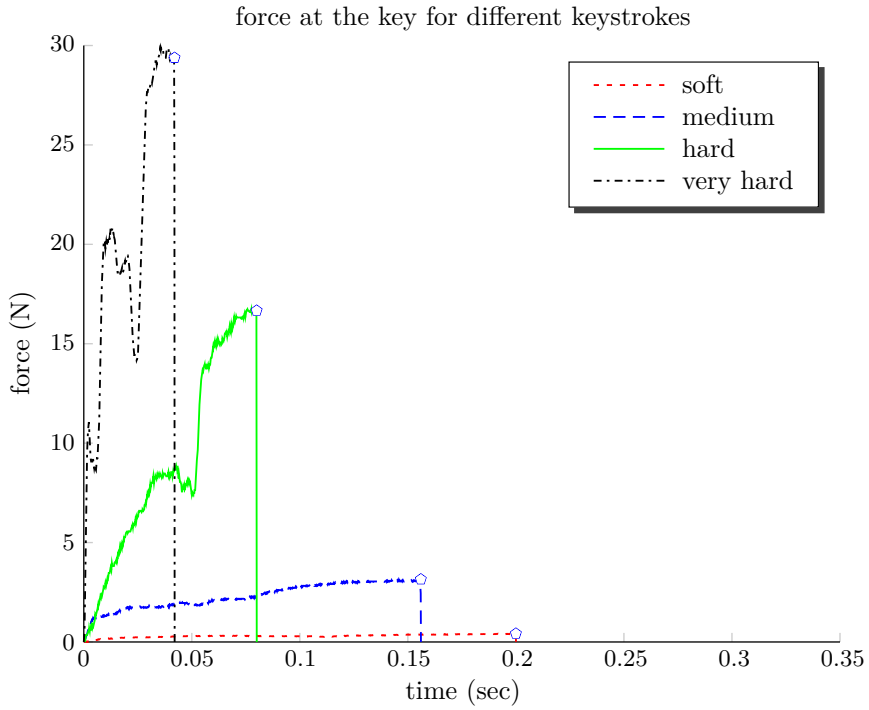

Figure 2-10: measurement of force at the keytip for different pressed keystrokes

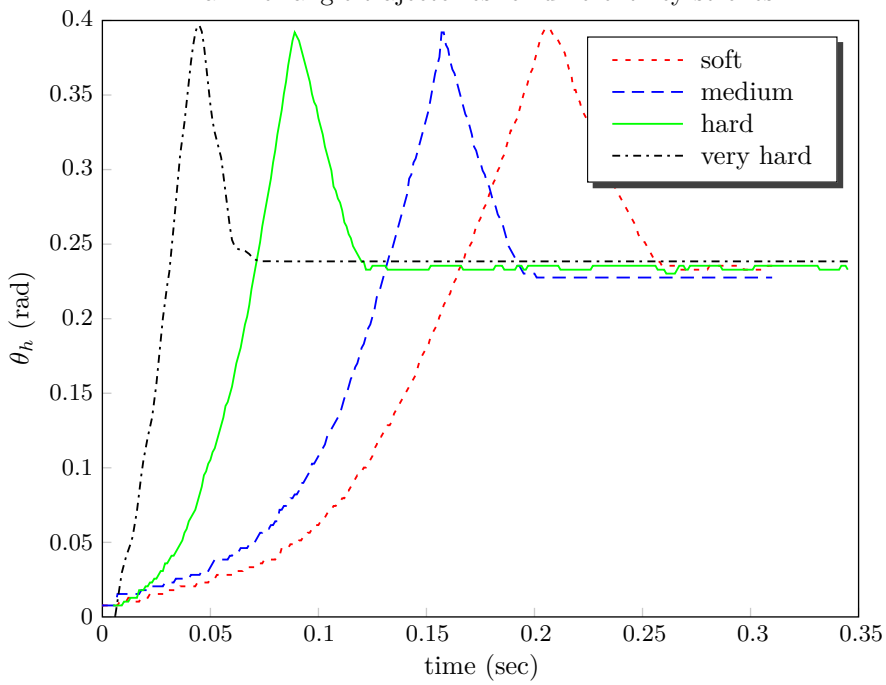

Figure 2-11: measurement of hammer trajectory for different pressed keystrokes

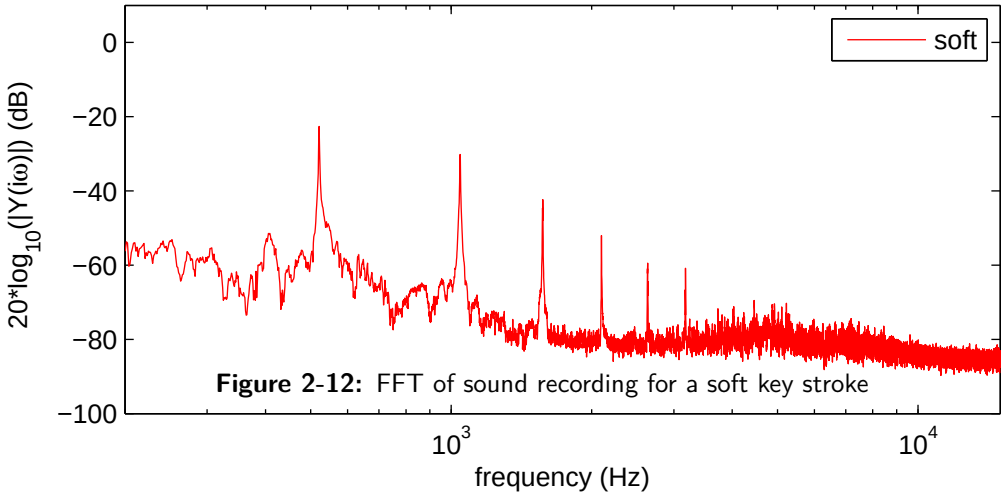

Figure 2-12: FFT of sound recording for a soft key stroke

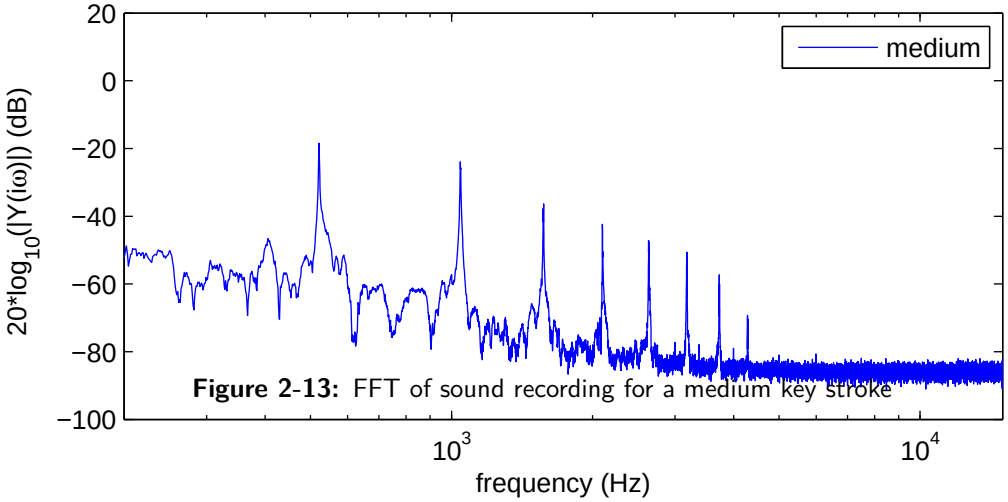

Figure 2-13: FFT of sound recording for a medium key stroke

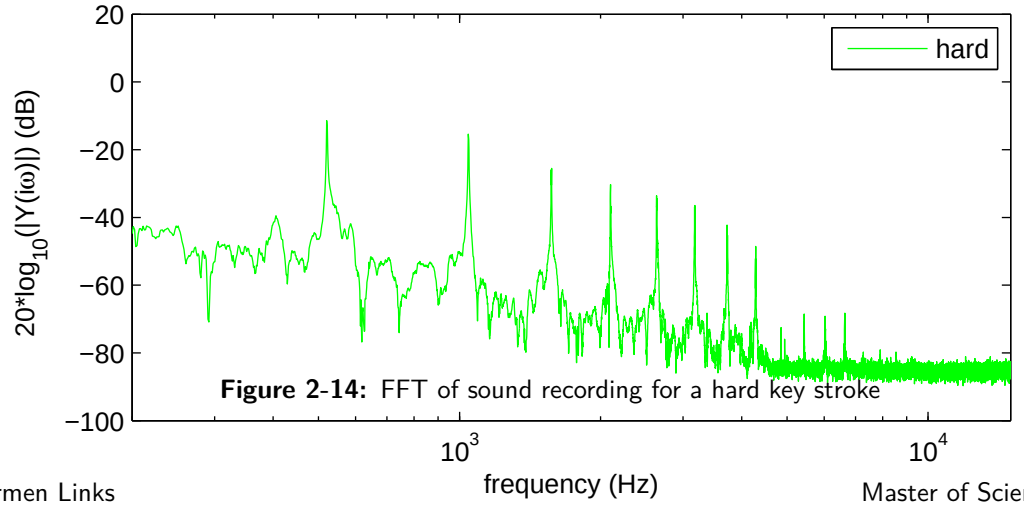

Figure 2-14: FFT of sound recording for a hard key stroke

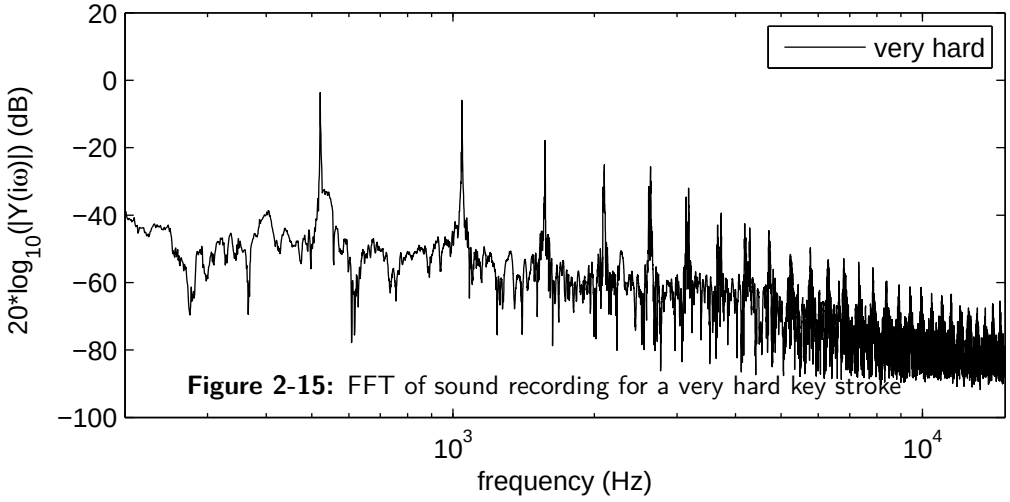

Figure 2-15: FFT of sound recording for a very hard key stroke

Chapter 3

Dynamical model

It is chosen to develop a dynamical model of the mechanism using a multi body modeling technique where the parts of the mechanism are represented with rigid bodies and the contact between the bodies is modeled as partly rigid contacts and partly custom made force equations. As opposed to system identification techniques, with a multi body model structure it is relatively easy to implement realistic configuration properties as parameters that can be adjusted. This is wanted because it is aimed for to develop a dynamical model where regulation settings and physical properties like the mass of the bodies appear as parameters. Next to the model for the mechanism, also a string model will be developed that can be combined with the mechanism model to be able to relate workings of the mechanism to the produced tone.

This chapter will explain the steps that are made to derive a multi body dynamical model of the mechanism and the string model. In the first paragraph, the configuration with five bodies in a two dimensional plane is presented. In paragraph two the dynamical equations of motion are derived, the bodies are represented by there center of mass coordinates and the equations are expressed in terms of the rotation angles of the bodies as generalized coordinates. For this the method of Lagrange's equation is used. In the third paragraph additional holonomic constraints are added to the equations of motion with Lagrange multipliers to account for the contact between the bodies. This results in a set of differential algebraic equations that can not be solved in a straight forward manner. An iterative method with the Gaus-Newton algorithm is used for this. Paragraph four explains the method with a hybrid automata that is used to deal with the changing configuration of the mechanism during operation. The hybrid automata is used to select subset of constraint equations that corresponds to the configuration of the mechanism during one particular motion stage. The fifth paragraph describes the force equations that are used to add elasticity and damping to some of the contacts. Also a force equation for the coupling between the mechanism and string model is given. In the last paragraph the details on the string model are given.

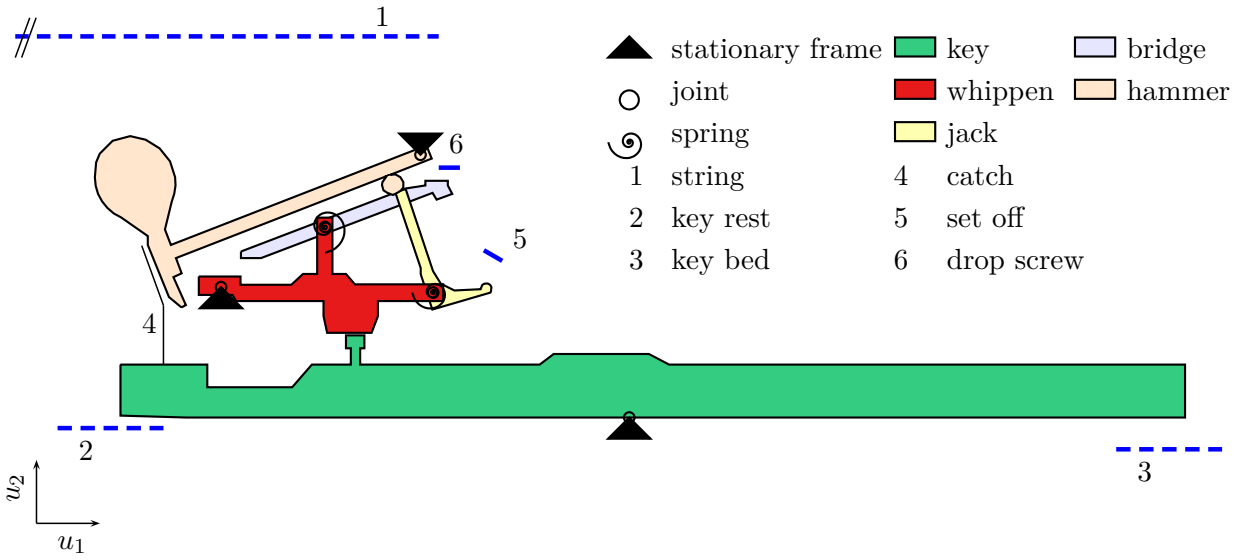

Figure 3-1: five bodies of a one key setup with names, joint locations, springs and stationary parts included in the configuration of the model

3-1 Configuration

The five bodies of the action mechanism that are included in the configuration of the dynamical model are shown in figure 3-1 as key (green), whippen (red), jack (jellow), bridge (purple) and hammer (orange). Although the rotation of the different parts remain relatively small during operation, it is chosen to take the rotation angles of the bodies as degrees of freedom for the model because this is also the case in real life. The bodies rotate about the fixed joints with locations indicated in figure 3-1. The figure also shows the location of two rotational springs on bridge and jack joints and six numbered stationary parts that impose constraints on the rotation of the bodies. Because the mechanism is constructed to operate in a 2 dimensional plane and the construction is very stiff in the direction perpendicular to this plane it suffices to represent the bodies in 2 dimensions. The bodies are constructed as a set of points that are located at rotational joints, contacts with other bodies or stationary parts and center of mass of the body. This is shown in figure 3-2 for one of the bodies. The position coordinates of the points on the bodies are expressed as (3-1).

$$\boldsymbol{u}_k(\theta_x) = \boldsymbol{u}_0 + \boldsymbol{\nu}_k(\theta_x) \tag{3-1}$$

In this equation the subscript $k = \{1, ..N\}$ is to number the points on the body and the subscript x for the angles θ_x is meant to discriminate between the different bodies with $x \in \{k, w, j, b, h\}$ for key, whippen, jack,bridge and hammer. The vector $\boldsymbol{u}_0$ is the fixed distance to the origin of a global axis $\{u_1, u_2\}$ and $\boldsymbol{\nu}_k(\theta_x)$ gives the position with respect to the joint of the body as a function of the rotation angle θ_x as (3-2). The vector $\boldsymbol{\xi}_k$ gives the rigidly constrained distances between point k and the joint on the local axis $\{\xi_1, \xi_2\}$.

$$\boldsymbol{\nu}_k(\theta_x) = \boldsymbol{R}(\theta_x)\boldsymbol{\xi}_k = \begin{pmatrix} cos(\theta_x) & sin(\theta_x) \\ -sin(\theta_x) & cos(\theta_x) \end{pmatrix} \begin{pmatrix} \xi_1 \\ \xi_2 \end{pmatrix}_k \tag{3-2}$$

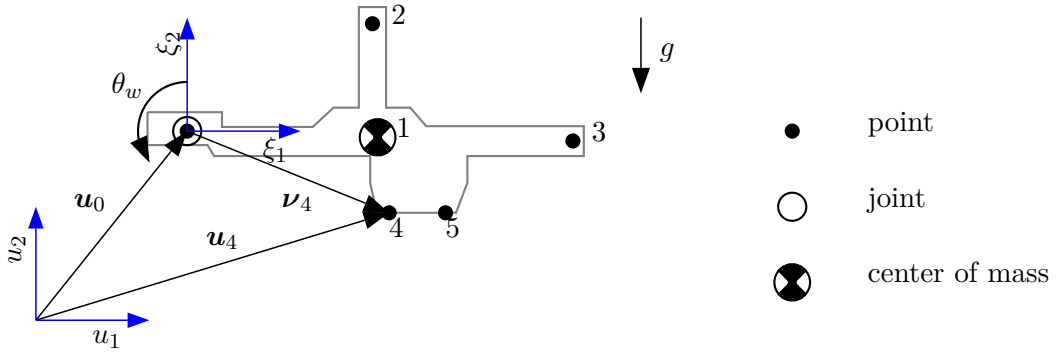

Figure 3-2: one of the bodies with numbering of the points and the position vector for point nr. 4 as an example

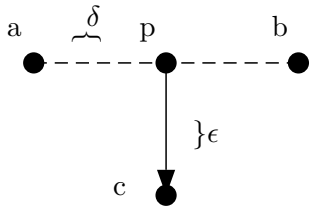

Figure 3-3: contacts between bodies as the shortest distance between a line defined by two points *a* and *b* on one body and a point *c* on another body. When the bodies make contact the constraint $\epsilon = 0$ is satisfied

For the dynamical equations each body will be represented by a scalar rotational inertia that is located at the center of mass of the body. The center of mass is defined as the mean location of the mass of a body. It is assumed that the mass is uniformly distributed which gives that the center of mass of a body equals its geometric center. An approximation of the center of mass is calculated for each body by dividing the body in to small segments for which the geometric center can be calculated more easy. Then the mean value is taken with a weight for the area of the segments. The rotational inertia that is located at the center of mass will be derived experimentally in chapter 4.

A one key configuration of the action mechanism in Figure 3-4 shows the locations where bodies make contact with each other or with stationary parts. So that next to the constraints for the joint locations, the bodies are also constrained by the contact locations as indicated with c_1 to c_{10}. These contacts are described by the shortest distance between a point on one body and a line defined by two points at another body. This shortest distance is given by the magnitude of a normal vector from the line to the point as drawn in figure 3-3. The table below names all contacts that are described by the pair $\{\epsilon_i, \delta_i\}$. The additional constraints ϵ_i are calculated as (3-3). This calculation involves a cross-product that is defined as (3-5). The length of the line segment from a to point p is calculated as δ_i in (3-4), the time derivative of δ_i is used in paragraph 3-5 as the sliding velocity between parts. The constraints ϵ_i are in

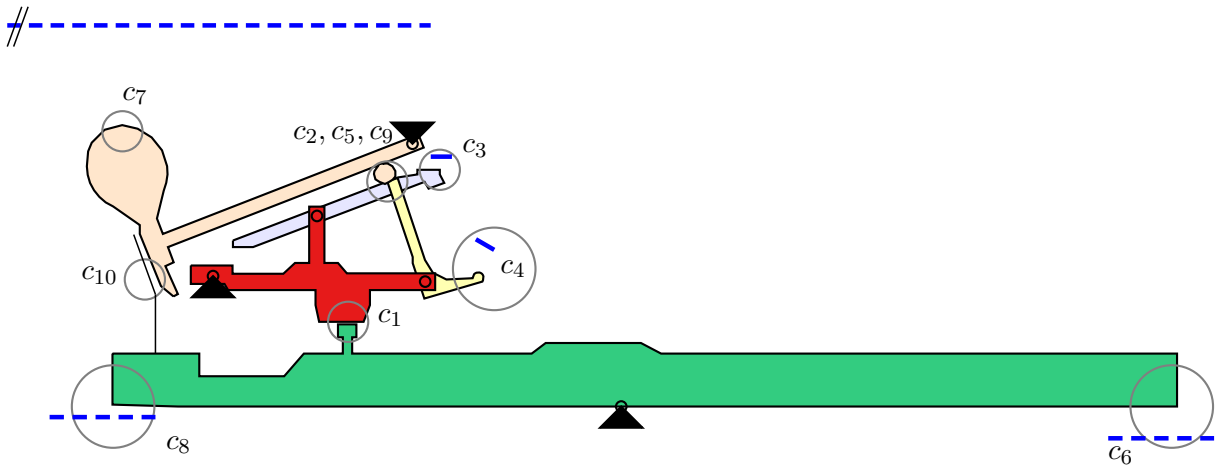

Figure 3-4: contacts between bodies and between bodies and stationary parts indicated with circles. These contacts c_1 to c_{10} impose constraints on the bodies

general not satisfied by a combination of the given generalized coordinates which means that they have to be provided explicitly to describe a configuration.

$c_1 - \{\epsilon_1, \delta_1\}$	capstan - whippen
$c_2 - \{\epsilon_2, \delta_2\}$	hammer - jack
$c_3 - \{\epsilon_3, \delta_3\}$	bridge - dropscrew
$c_4 - \{\epsilon_4, \delta_4\}$	jacktoe - set off button
$c_5 - \{\epsilon_5, \delta_5\}$	jack - bridge
$c_6 - \{\epsilon_6, \delta_6\}$	key - key bed
$c_7 - \{\epsilon_7, \delta_7\}$	hammer - string
$c_8 - \{\epsilon_8, \delta_8\}$	key - key rest
$c_9 - \{\epsilon_9, \delta_9\}$	bridge - jack
$c_{10} - \{\epsilon_{10}, \delta_{10}\}$	hammer - catch

$$\epsilon_i = \frac{(\boldsymbol{b} - \boldsymbol{a}) \times (\boldsymbol{a} - \boldsymbol{c})}{||\boldsymbol{b} - \boldsymbol{a}||} = 0 \tag{3-3}$$

$$\delta_i = \sqrt{(\boldsymbol{a} - \boldsymbol{c})^2 - \epsilon_i^2} \tag{3-4}$$

$$\boldsymbol{A} \times \boldsymbol{B} = det \begin{pmatrix} \boldsymbol{i} & \boldsymbol{j} & \boldsymbol{k} \\ a_1 & a_2 & 0 \\ b_1 & b_2 & 0 \end{pmatrix} = a_1 b_2 - a_2 b_1 \tag{3-5}$$

3-2 Equations of motion

To construct the equations of motion, the method of Lagrange's equations is used. First expressions for the potential and kinetic energy of the system are set up and the equations of motion are expressed in terms of the generalized coordinates which are defined as the the rotation angles of the bodies as (3-6).

$$\boldsymbol{q} = \begin{pmatrix} q_1 & \dots & q_5 \end{pmatrix}^T = \begin{pmatrix} \theta_k & \theta_w & \theta_j & \theta_b & \theta_h \end{pmatrix}^T \tag{3-6}$$

The kinetic energy T of one body consists of the sum of a rotational and translational part as (3-7). With the translational part in both vertical and horizontal direction.

$$T = \underbrace{\frac{1}{2} I \dot{\theta}^2}_{rotational} + \underbrace{\frac{1}{2} \sum_{i=1}^{2} m \dot{u}_i^2}_{translational} \tag{3-7}$$

The total kinetic energy is the sum of kinetic energies of the separate bodies given in (3-8). Here the rotational part depends on the rotational inertia I_k and rotational velocity $\dot{q}_k$, while the translational part depends on the mass m_k of the body and translational velocity $\dot{u}_{i,k}$ with $i \in \{1, 2\}$ as an index for horizontal and vertical direction and $k \in \{1, 2, 3, 4, 5\}$ as the index for different bodies.

$$T(\dot{\boldsymbol{q}}, \boldsymbol{q}) = \frac{1}{2} \sum_{k=1}^{5} (I_k \dot{q}_k^2 + \sum_{i=1}^{2} m_k \dot{u}_{i,k}^2(\dot{\boldsymbol{q}}, \boldsymbol{q})) \tag{3-8}$$

The potential energy V of one body consists of elastic and gravity related potential as (3-9). The potential energy is constructed so that $\frac{\partial V}{\partial \boldsymbol{q}_k} = -F_k$, which means that the elastic and gravitational forces F_k derive from a potential.

$$V = \underbrace{V_e}_{elastic} + \underbrace{mgu_2}_{gravitational} \tag{3-9}$$

The springs on the bridge and jack shown in figure 3-1 are modeled as rotational springs in the joints of the bodies with a potential as (3-10) with stiffness coefficient k. This corresponds to a spring that obeys Hooks law $F_{spring} = k\theta = -\frac{\partial V}{\partial \theta}$.

$$V_{spring} = \frac{1}{2} k \theta^2 \tag{3-10}$$

(3-11) gives the total potential energy with V_e as the elastic potential of the two rotational springs and the second term as the gravitation potential with $u_{2,k}(\boldsymbol{q})$ as the vertical component of the center of mass coordinates.

$$V(\boldsymbol{q}) = V_e(\boldsymbol{q}) + \sum_{k=1}^{5} g m_k u_{2,k}(\boldsymbol{q}) \tag{3-11}$$

With the constructed energy functions, Lagrange's equations are set up to derive the equations of motion as (3-12). $\boldsymbol{Q}^{ncons}$ represents the non conservative forces consisting of the external force on the key and dissipation forces caused by damping. This set of equations is computed symbolically with the use of Matlab, the code is given in the appendix.

$$\frac{d}{dt}\frac{\partial T}{\partial \dot{\boldsymbol{q}}} - \frac{\partial T}{\partial \boldsymbol{q}} + \frac{\partial V}{\partial \boldsymbol{q}} - \boldsymbol{Q}^{ncons} = 0 \tag{3-12}$$

The resulting set of differential equations can be partitioned as (3-13).

$$\boldsymbol{f}_{tot}(\ddot{\boldsymbol{q}}, \dot{\boldsymbol{q}}, \boldsymbol{q}) = \boldsymbol{f}_T(\ddot{\boldsymbol{q}}, \dot{\boldsymbol{q}}, \boldsymbol{q}) + \boldsymbol{f}_V(\boldsymbol{q}) + \boldsymbol{Q}(\dot{\boldsymbol{q}}, \boldsymbol{q}) = 0 \tag{3-13}$$

Now to arrive at a description that can be used to solve for the accelerations $\ddot{\boldsymbol{q}}$, a mass matrix $\boldsymbol{M} = \frac{\partial \boldsymbol{f}_T}{\partial \ddot{\boldsymbol{q}}}$ is introduced and the velocity and position dependent forces are added to one generalized forces vector $\boldsymbol{f}(\dot{\boldsymbol{q}}, \boldsymbol{q}) = \boldsymbol{f}_{tot} - \boldsymbol{M}\ddot{\boldsymbol{q}}$, this gives (3-14).

$$\boldsymbol{M}(\boldsymbol{q})\ddot{\boldsymbol{q}} = \boldsymbol{f}(\dot{\boldsymbol{q}}, \boldsymbol{q}) \tag{3-14}$$

3-3 Constraint equations of motion

The set of m additional holonomic constraint equations that were given in paragraph 3-1 as ϵ_i are gathered in a column vector (3-15). For each configuration of the mechanism, a subset of the constraints is active. This is indicated with a sub-script i on the vector with constraints $\boldsymbol{D}_{(i)}$. The different subsets will be given in the next chapter.

$$\boldsymbol{D}(\boldsymbol{q}) = \begin{pmatrix} \epsilon_1 & \epsilon_2 & ... & \epsilon_m \end{pmatrix}^T \tag{3-15}$$

The constrains are combined with (3-14) and a vector $\boldsymbol{\lambda}$ with m Lagrange multipliers is introduced in the equation so that the constraint equations of motion are given as (3-16). Here $\boldsymbol{\Phi} = \frac{\partial \boldsymbol{D}}{\partial \boldsymbol{q}}$ and $\boldsymbol{\Phi}^T\boldsymbol{\lambda}$ gives the unknown forces in the direction of the constraints. The Jacobian matrix $\boldsymbol{\Phi}$ has dimensions $m \times n$ with n the number of generalized coordinates. Because $m \neq n$ the matrix $\boldsymbol{\Phi}$ will be rank deficient, moreover it is assumed that $\boldsymbol{\Phi}$ will have linear independent rows because the constraints ϵ are uniquely defined.

$$\begin{gathered} \boldsymbol{M}(\boldsymbol{q})\ddot{\boldsymbol{q}} = \boldsymbol{f}(\dot{\boldsymbol{q}}, \boldsymbol{q}) - \boldsymbol{\Phi}_{(i)}^T(\boldsymbol{q})\boldsymbol{\lambda} \\ s.t\ \boldsymbol{D}_{(i)}(\boldsymbol{q}) = 0 \end{gathered} \tag{3-16}$$

This type of equations is a mixed set of Differential and Algebraic Equations (DAEs). A DAE can be characterized by a differential index which is defined as the number of times the equation has to be differentiated to obtain an ODE. A high index means that the complexity of numerical integration increases drastically and there is no guaranty that the equations are solvable [24,27,28]. It is aimed for to arrive at a system of equations that can be solved in Matlab. Currently, only index 1 DAEs can be solved in Matlab using a standard ODE solver, however (3-16) appears to be of index 3. Hereby it is necessary to convert (3-16) to a set of equivalent ODEs or index 1 DAEs.

It is possible to apply a coordinate transformation that maps $\boldsymbol{q}$ to a set of kinematic admissible coordinates so that no explicit constraint are needed. This method gives a set of ODEs that can be solved in Matlab. This has a drawback that for every possible configuration, a set of equations with kinematic admissible coordinates has to be calculated. Because of this drawback, it is chosen to use a method so that (3-16) can be solved as a set of index 1 DAEs. The constraints are differentiated twice with respect to time i.e. twice the full derivative like (3-17).

$$\frac{d\boldsymbol{D}(\boldsymbol{q})}{dt} = \frac{\partial \boldsymbol{D}}{\partial \boldsymbol{q}}\frac{d\boldsymbol{q}}{dt} = \boldsymbol{\Phi}\dot{\boldsymbol{q}} \quad \frac{d^2\boldsymbol{D}(\boldsymbol{q})}{dt^2} = \frac{\partial(\boldsymbol{\Phi}\dot{\boldsymbol{q}})}{\partial \boldsymbol{q}}\dot{\boldsymbol{q}} + \boldsymbol{\Phi}\ddot{\boldsymbol{q}} \tag{3-17}$$

Now the differentiated constraints can be combined with the force equations as a system of equations (3-18) which is a set of index 1 DAEs that can be solved for the accelerations $\ddot{\boldsymbol{q}}$ and Lagrange multipliers $\boldsymbol{\lambda}$ simultaneously. To be able to solve (3-18) the left hand side matrix has to be non-singular, hence $\boldsymbol{\Phi}^T\boldsymbol{\Phi}$ must be non-singular. This will always be the case because $\boldsymbol{\Phi}$ has full row rank. A drawback of (3-18) is that the constraints no longer apply to positions but only on accelerations. This results in a numerical drift when a solution is computed with numerical time integration.

$$\begin{pmatrix} \boldsymbol{M}(\boldsymbol{q}) & \boldsymbol{\Phi}^T(\boldsymbol{q}) \\ \boldsymbol{\Phi}(\boldsymbol{q}) & 0 \end{pmatrix} \begin{pmatrix} \ddot{\boldsymbol{q}} \\ \boldsymbol{\lambda} \end{pmatrix} = \begin{pmatrix} \boldsymbol{f}(\boldsymbol{q}, \dot{\boldsymbol{q}}) \\ -\frac{\partial(\boldsymbol{\Phi}\dot{\boldsymbol{q}})}{\partial \boldsymbol{q}}\dot{\boldsymbol{q}} \end{pmatrix} \tag{3-18}$$

3-4 Constraint stabilization

As mentioned in the previous paragraph, when numerically integrating the system of equations (3-18) a problem arises because after differentiating (3-15) twice, the constraints no longer apply to the positional configuration of the bodies but only on the accelerations. This causes that the set of DAEs is unstable from a computational point of view and this results in a numerical drift on the position and velocity variables. That is, the computed solution drifts away from the subset of the state-space where the constraints are satisfied. Or in other words, the solution drifts away from the kinematic admissible coordinate values. This numerical drift is related to round off errors and depends on the used integration method.

This is a problem that arises frequently in multi body dynamics modeling, there are different methods to deal with this problem. The most often used method is Baumgard stabilization, with this method the acceleration constraint $\ddot{\boldsymbol{D}} = 0$ is augmented to $\ddot{\boldsymbol{D}} + \alpha\dot{\boldsymbol{D}} + \beta\boldsymbol{D} = 0$ and the parameters α and β are chosen such that the characteristic equation has zeros in the LHP. A problem with this method is that the parameters have to be chosen according to the configuration [31]. When $\boldsymbol{D}$ changes, new values for α and β can be necessary. For this reason another method is used that does not require any parametrization that depends on the configuration. This method is called a projection method [19,31] and is also referred to as post-stabilization [29] and perturbation method [30].

The projection method has an advantage over other methods because it does not require a change in coordinates or some additional terms in the equations of motion. Before each time integration step, the numerical solution $(\dot{\boldsymbol{q}}_n\ \boldsymbol{q}_n)$ is corrected iteratively so that $\dot{\boldsymbol{D}} = 0$ and $\boldsymbol{D} = 0$ are satisfied. The problem is handled as an optimization problem with equality constraint written as (3-19).

$$\begin{aligned} \tilde{\dot{\boldsymbol{q}}}_n &= argmin\,||\tilde{\dot{\boldsymbol{q}}}_n - \dot{\boldsymbol{q}}_n|| \quad subject\ to\ \ \dot{\boldsymbol{D}}(\boldsymbol{q}_n) = 0 \\ \tilde{\boldsymbol{q}}_n &= argmin\,||\tilde{\boldsymbol{q}}_n - \boldsymbol{q}_n|| \quad subject\ to\ \ \boldsymbol{D}(\boldsymbol{q}_n) = 0 \end{aligned} \tag{3-19}$$

The calculated coordinate vector $(\dot{\boldsymbol{q}}_n\ \boldsymbol{q}_n)$ is corrected for the velocities with $\delta\dot{\boldsymbol{q}}_n = \tilde{\dot{\boldsymbol{q}}}_n - \dot{\boldsymbol{q}}_n$ and for the positions with $\delta\boldsymbol{q}_n = \tilde{\boldsymbol{q}}_n - \boldsymbol{q}_n$. For the velocities this problem can be solved in one step with the least squares solution (3-20) and for the positions the same projection can be used iteratively wich is refered to as the Gauss-Newton algorithm.

$$\tilde{\dot{\boldsymbol{q}}}_n = \dot{\boldsymbol{q}}_n - \boldsymbol{\Phi}^T(\boldsymbol{\Phi}\boldsymbol{\Phi}^T)^{-1}\dot{\boldsymbol{D}} \tag{3-20}$$

$$\tilde{\boldsymbol{q}}_n = \boldsymbol{q}_n - \boldsymbol{\Phi}^T(\boldsymbol{\Phi}\boldsymbol{\Phi}^T)^{-1}\boldsymbol{D} \tag{3-21}$$

3-5 Constraints switching

A hybrid automata is used to deal with the switching between the additional holonomic constraints when parts make or break contact. The hybrid automata as shown in figure 3-5 gives the workings with four motion stages as described in chapter 2. And to capture the different configurations of the mechanism additional sub-schemes are setup for stage II, III and IV. The circles represent the motion stages with the active set of constraint indicated with the sub index. The arrows are unique one way transitions between these stages defined by a transition function g.

Most transition functions are zero crossings of one of the inactive constraints ϵ, but also constraint forces are used as transition from I to II and from IV to II. When an input force is applied at the key, the active stage switches from I or IV to stage II when the force in the key joint that is caused by the force that is applied at the key tip is bigger than the constraint force in the key joint wich is caused by gravity on the action parts.

The sets of constraints and transition functions per stage are given in the tables below.

stage	*sets of constraints*	*description*
I rest	$\boldsymbol{D}_{(11)} = \{\epsilon_1, \epsilon_2, \epsilon_8\ \}$	all bodies are in rest
II$^{(1)}$ acceleration	$\boldsymbol{D}_{(21)} = \{\epsilon_1, \epsilon_2\ \}$	hammer is accelerated
II$^{(2)}$ acceleration	$\boldsymbol{D}_{(22)} = \{\epsilon_1, \epsilon_2, \epsilon_3\ \}$	bridge in contact with drop screw
III$^{(1)}$ let off	$\boldsymbol{D}_{(31)} = \{\epsilon_1, \epsilon_4\ \}$	jack in contact with set off and hammer is released
III$^{(2)}$ let off	$\boldsymbol{D}_{(32)} = \{\epsilon_1, \epsilon_4, \epsilon_9\ \}$	side of jack in contact with bridge
III$^{(3)}$ let off	$\boldsymbol{D}_{(33)} = \{\epsilon_1, \epsilon_4, \epsilon_6\ \}$	key in contact with key bed
III$^{(4)}$ let off	$\boldsymbol{D}_{(34)} = \{\epsilon_1, \epsilon_4, \epsilon_6, \epsilon_9\ \}$	side of jack in contact with bridge and key in contact with key bed
IV$^{(1)}$ catch	$\boldsymbol{D}_{(41)} = \{\epsilon_1, \epsilon_2, \epsilon_6\}$	key is released
IV$^{(2)}$ catch	$\boldsymbol{D}_{(42)} = \{\epsilon_1, \epsilon_4, \epsilon_5, \epsilon_6\ \}$	hammer is in contact with bridge
IV$^{(3)}$ catch	$\boldsymbol{D}_{(43)} = \{\epsilon_1, \epsilon_5, \epsilon_6, \epsilon_{10}\ \}$	hammer is caught
IV$^{(4)}$ catch	$\boldsymbol{D}_{(44)} = \{\epsilon_1, \epsilon_5, \epsilon_6, \epsilon_{10}\ \}$	key touches key bed

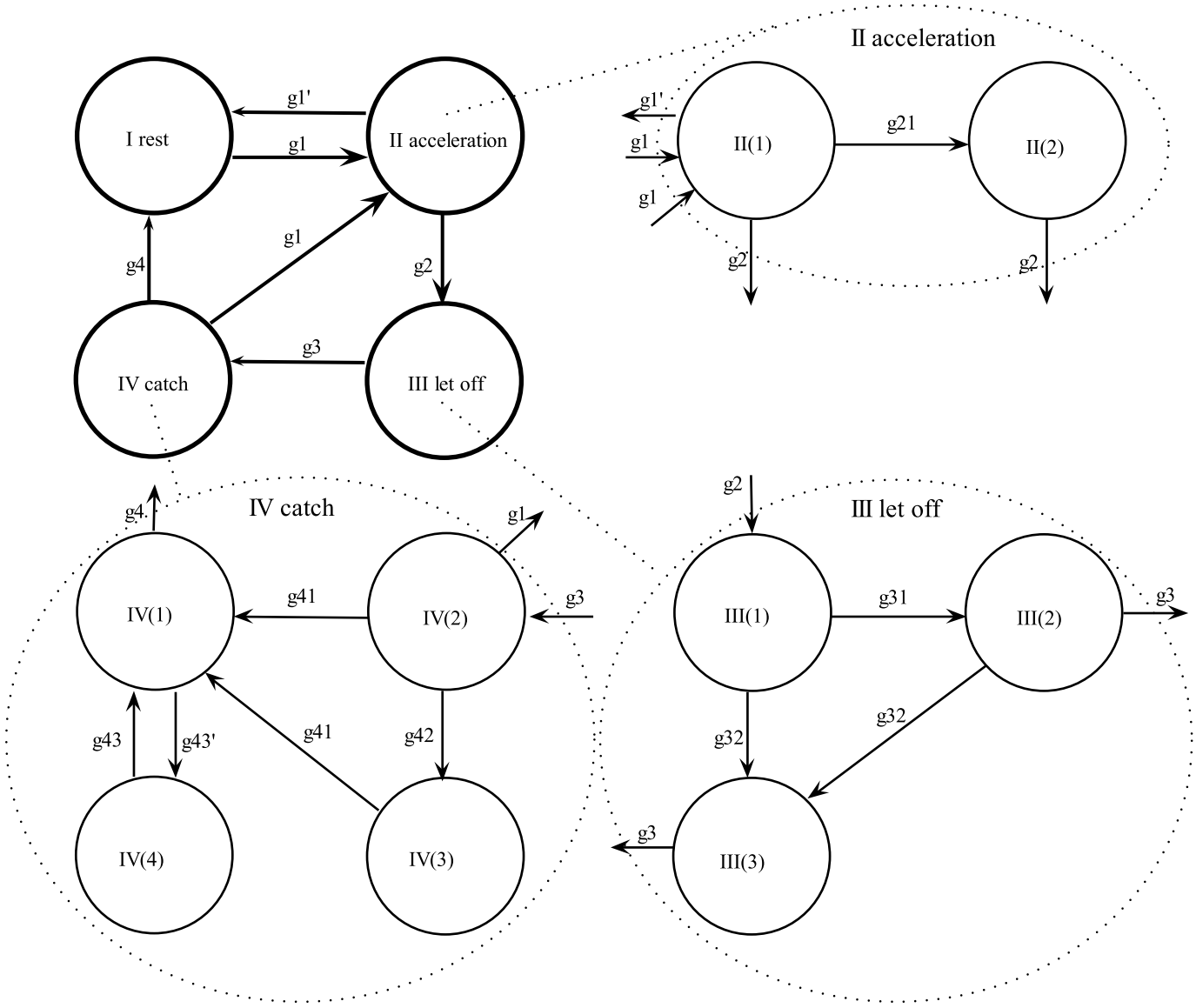

Figure 3-5: automata for switching subsets of the constraints, the stages I,II,III and IV correspond to the stages that were explained in chapter 2-1 with figure 2-2

transition function	*description*
$g_1 = u - R_k(q) = 0$	u equals constraint force in the key joint
$g_1' = u = 0$	key is released
$g_2 = \epsilon_4 = 0$	jacktoe hits set off button
$g_{21} = \epsilon_3 = 0$	bridge hits drop screw
$g_{31} = \epsilon_9 = 0$	jack hits side of the bridge
$g_{32} = \epsilon_6 = 0$	key hits key bed
$g_3 = \epsilon_7 = 0$	hammer hits string
$g_{41} = \epsilon_{10} = 0$	hammer back hits catch
$g_{42} = \epsilon_5 = 0$	key is released
$g_{43} = \epsilon_8 < 0$	key hitskey rest
$g_{43'} = \epsilon_8 > 0$	key bounces back
$g_4 = \epsilon_8 = 0$	key stays on key rest

3-6 Contact dynamics

An attempt has been made to model the contact between parts at locations given in figure 3-3 with a combination of hard constraints as given in (3-15) when the parts remain in contact and additional forces for contacts with elasticity and damping. When a contact force has to be added to the equations of motion, this can be done by multiplying the magnitude of the custom made force with the direction vector that is associated with the constraint of the contact. This gives a force in the direction of the particular constraint expressed in terms of the degrees of freedom. This can be extracted from the vector with generalized forces so that this gives (3-22). The sub index i corresponds to the active set of hard constraints so that $\frac{\partial \boldsymbol{D}_{(i)}}{\partial \boldsymbol{q}} = \boldsymbol{\Phi}_{(i)}$ and k for the constraint that is associated with $\boldsymbol{f}_{contact}$.

$$\begin{pmatrix} \boldsymbol{M} & \boldsymbol{\Phi}_{(i)}^T \\ \boldsymbol{\Phi}_{(i)} & 0 \end{pmatrix} \begin{pmatrix} \ddot{\boldsymbol{q}} \\ \boldsymbol{\lambda} \end{pmatrix} = \begin{pmatrix} \boldsymbol{f} - \boldsymbol{\Phi}_{(k)}^T \boldsymbol{f}_{contact} \\ -\frac{\partial (\boldsymbol{\Phi}_{(i)} \dot{\boldsymbol{q}})}{\partial \boldsymbol{q}} \dot{\boldsymbol{q}} \end{pmatrix} \tag{3-22}$$

The contact points whippen - capstan, jack - hammerknuckle and hammer-catch can slide over each other while remaining in contact during operation. This causes sliding friction between the parts. Sliding friction is a very complex phenomenon that is in general hard to model [32]. An often used model to approximate this friction is the Coulomb friction model. With this model the friction force is modeled as a force that depends on the normal force between the parts trough a constant coefficient μ_c and is independent of the magnitude of the relative tangential sliding velocity $\dot{\delta}$. This sliding velocity is only used for the direction of the force. With a normal force that results from a deformation ϵ (3-23) gives the friction force.

$$f_d = f_d(\epsilon, \dot{\delta}) = \begin{cases} \mu_c f_n(\epsilon) & \text{for } \dot{\delta} < 0 \\ < \mu_c f_n(\epsilon) \text{ and } > -\mu_c f_n(\epsilon) & \text{for } \dot{\delta} = 0 \\ -\mu_c f_n(\epsilon) & \text{for } \dot{\delta} > 0 \end{cases} \tag{3-23}$$

The discontinuity for a change of sign of $\dot{\delta}$ in (3-23) can give problems in simulation, because of this a smooth equation that approximates the Coulomb friction model can be used as (3-24). with $f_c(\dot{\delta})$ a function as shown in figure 3-4. Here $\dot{\delta}_c$ is a constant that has to be determined experimentally. Although the main reason to implement a smooth function like $f_c(\dot{\delta})$ is to avoid the discontinuity in the calculation of the forces, it can be argued that this actually describes the sliding friction in a way that is closer to the physical phenomenon.

$$f_d(\epsilon, \dot{\delta}) = -\mu_c f_n(\epsilon) f_c(\dot{\delta}) \tag{3-24}$$

A 3th order polynomial equation (3-25) is used to model the normal force f_n for felt material. This equation was given in [5,8] to characterize the dynamical behavior of felt. In [5] the coefficient a_2 is taken as a negative value which makes it arguable that the second order term is left out.

$$f_n(\epsilon, \dot{\epsilon}) = (a_3\epsilon^3 + a_2\epsilon^2 + a_1\epsilon)(1 - d\dot{\epsilon}) \tag{3-25}$$

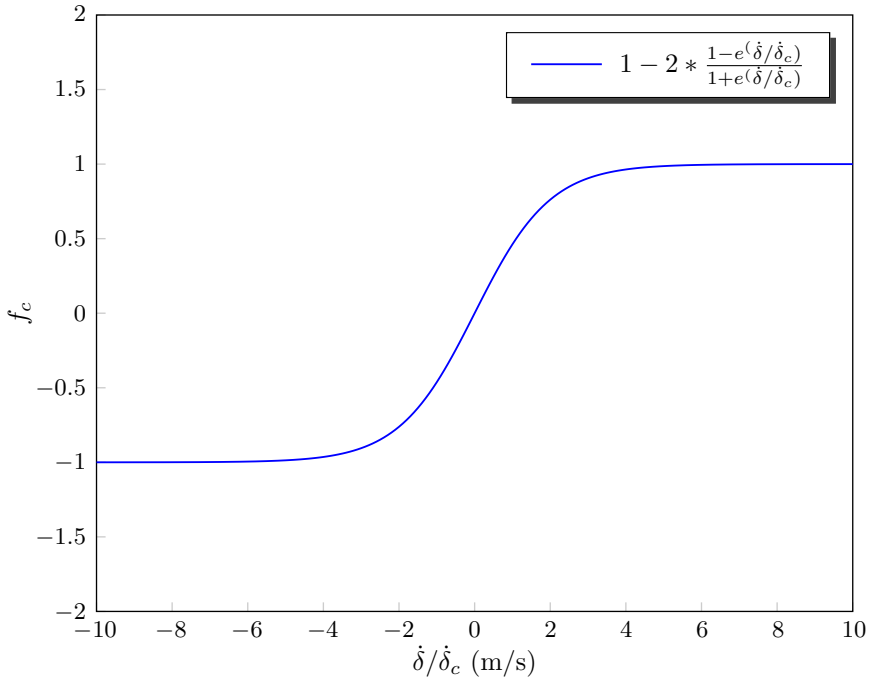

Figure 3-6: function f_c to approximate Coulomb friction for the sliding friction between contacts

A model for the contact between hammer and string (3-26) is given by Hall in [16]. With uh_3 the vertical component of the hammer tip coordinates and η as the vertical component of the contact part of the string which depends on the dynamical behavior of the string trough the horizontal component of the contact part of the string a and time t. Basically this equation is a nonlinear expression for the stiffness of the felt material of the hammerhead with stiffness coefficient k and exponent p. With typical values of p between 2 and 5. And η is a solution to a dynamical equation for the string displacement.

$$f_{hs} = k\,|uh_3 - \eta(a,t)|^p \tag{3-26}$$

3-7 String model

An approximation of transverse vibration in a string can be modeled with an extension of the standard wave equation in 1D as (3-27). This PDE is also used in [8] and [26].

In this equation the second order derivative in the time variable represents the acceleration force in the string with μ as the mass-density coefficient. This term provides a restoring force in the string that is caused by the string tension with linear tension coefficient T. The fourth order derivative in the space variable represents the elasticity force in the string due to bending stiffness with Youngs modulus E and moment of inertia I. This term is also used in structural dynamics for modeling clamped beams and causes enharmonic vibrations.

Because for piano strings it holds that $T >> EI$ the partials will be harmonic frequencies that are multiples of the ground frequency as with a fully elastic string but slightly shifted due to the fourth order term. The other two terms on the left hand side of the equation

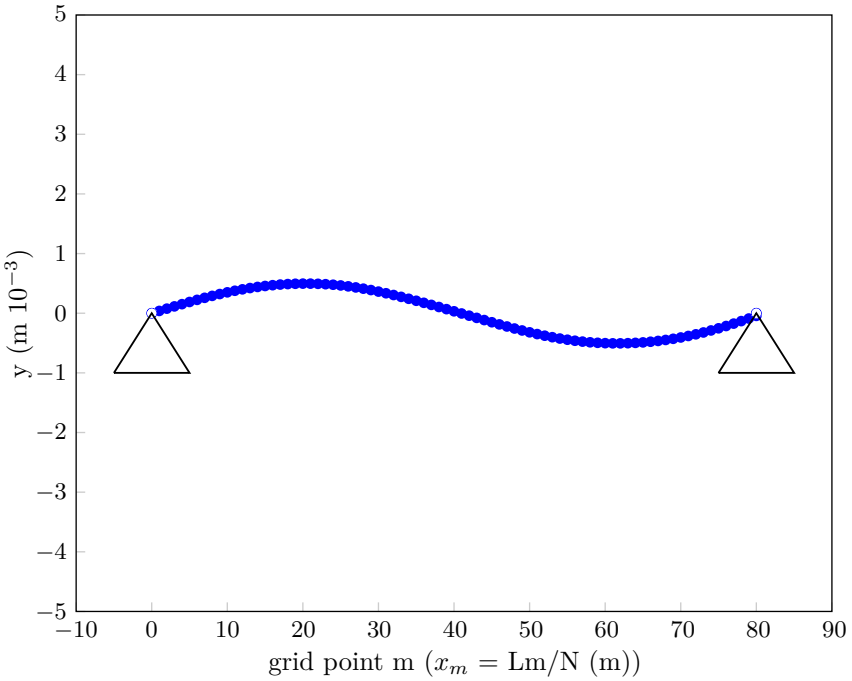

Figure 3-7: visualisation of a vibrating string that is discretized on a horizontal grid

provide damping. The term with first order time derivative gives an exponential decay of the vibrations while term with the mixed time and space derivative is used to give frequency dependent damping, that is higher harmonic frequencies dampen out at a faster rate compared to lower harmonic frequencies. Originally in [8] this term was a third order partial derivative in the time variable but as some values for the damping coefficient can cause instability this term was replaced for the mixed one.

The force equation on the right hand side is the hammer-string interaction force as an input of the string model at impact location a.

$$\mu\frac{\partial^2 y}{\partial t^2} + EI\frac{\partial^4 y}{\partial x^4} - T\frac{\partial^2 y}{\partial x^2} + d_1\frac{\partial y}{\partial t} - d_2\frac{\partial^3 y}{\partial x^2 \partial t} = f(t)\delta(x-a) \tag{3-27}$$

A practical method to solve (3-27) is to discretize the equation in space using a finite difference scheme on a grid $x_m = m\Delta x$ with integer number $m \in [0, N]$ where N is the number of spatial grid points .

$$\begin{aligned}\frac{\partial^2 y}{\partial x^2} &= \frac{y_{m-1} - 2y_m + y_{m+1}}{\Delta x^2} + \mathcal{O}(\Delta x^2)\\ \frac{\partial^4 y}{\partial x^4} &= \frac{y_{m-2} - 4y_{m-1} + 6y_m - 4y_{m+1} - y_{m+2}}{\Delta x^4} + \mathcal{O}(\Delta x^4)\end{aligned} \tag{3-28}$$

$$\boldsymbol{A}_1 = \frac{1}{\Delta x^2}\begin{pmatrix} -2 & 1 & 0 & .. & .. & 0 \\ 1 & -2 & 1 & 0 & .. & 0 \\ : & : & : & : & : & : \\ : & : & : & : & : & : \\ 0 & .. & 0 & 1 & -2 & 1 \\ 0 & .. & .. & 0 & 1 & -2 \end{pmatrix} \tag{3-29}$$

$$\boldsymbol{A}_2 = \frac{1}{\Delta x^4}\begin{pmatrix} 6 & -4 & -1 & 0 & .. & .. & 0 \\ -4 & 6 & -4 & -1 & 0 & .. & 0 \\ 1 & -4 & 6 & -4 & -1 & 0 & 0 \\ : & : & : & : & : & : & : \\ : & : & : & : & : & : & : \\ 0 & .. & 0 & 1 & -4 & 6 & -4 \\ 0 & .. & .. & 0 & 1 & -4 & 6 \end{pmatrix} \tag{3-30}$$

With the coefficient matrices (3-29) and (3-30), the wave equation reduces to a a set of N ODEs.

$$\mu\frac{\partial^2 \boldsymbol{y}}{\partial t^2} - (d_2\boldsymbol{A}_1 - d_1\boldsymbol{I})\frac{\partial \boldsymbol{y}}{\partial t} - (T\boldsymbol{A}_1 - EI\boldsymbol{A}_2)\boldsymbol{y} = \boldsymbol{f}(t)\delta(x-a) \tag{3-31}$$

With $\boldsymbol{x}_1 = \dot{\boldsymbol{y}}$ and $\boldsymbol{x}_2 = \boldsymbol{y}$ (3-31) can be written in state space with state vector $\boldsymbol{x} = (\boldsymbol{x}_1, \boldsymbol{x}_2)^T$.

$$\begin{pmatrix} \dot{\boldsymbol{x}}_1 \\ \dot{\boldsymbol{x}}_2 \end{pmatrix} = \begin{pmatrix} \frac{d_2}{\mu}\boldsymbol{A}_1 - \frac{d_1}{\mu}\boldsymbol{I} & \frac{T}{\mu}\boldsymbol{A}_1 - \frac{EI}{\mu}\boldsymbol{A}_2 \\ \boldsymbol{I} & 0 \end{pmatrix}\begin{pmatrix} \boldsymbol{x}_1 \\ \boldsymbol{x}_2 \end{pmatrix} + \begin{pmatrix} \frac{1}{\mu} \\ 0 \end{pmatrix}\boldsymbol{f}(t)\delta(x-a) \tag{3-32}$$

The output of the string model is taken as the grid point closest to the rigid boundary of the string model as being the termination at the bridge. According to ref [26] a good approximation of the force at the bridge is now $F_b(t) = -T\frac{\partial y}{\partial x}|_{x=L} = -T\frac{\partial y}{\partial x}|_{x=x2_{N-1}}$. This can be verified by the fact that the displacement in horizontal direction of a string segment is negligible compared to the vertical displacement.

Chapter 4

Parameter estimation

For both the model of the action mechanism and the string model developed in chapter 3, numerical values for some physical parameters have to be determined. The weight under gravity of the parts of the mechanism is easily measured with a scale weight. The rotational inertia of the different parts is derived from performed pendulum tests, together with the damping in the rotational joints. The parameters for the sliding friction in the model are tuned so that the trajectories of the different parts match measurements for a particular key stroke where the recorded force signal at the tip of the key is used as an input signal for the model. The tuning of the force equation for the hammer-string interaction is done with a fixed distance for the string hight and the stiffness coefficient and exponent are tuned so that the hammer trajectory matches the measurements for different keystrokes. After this, the hammer-string interaction force is used as an input for the string model and the string parameters are tuned to match the FFT of the measured sound for keystrokes with different intensity. The damping parameters of the string model are tuned so that the decay of the sound signal in the time domain matches the measurements.

4-1 Experiments and observations

A pendulum test has been performed for key, whippen, bridge and jack by connecting a thin wire to the part and determine the period of oscillation. With this period, the rotational inertia can be approximated and by applying Huygens-Steiners theorem for parallel axis, the rotational inertia about the center of mass can be derived for each part. For the hammer, a different test was setup. The hammer was rigidly clamped in vertical position, set with an initial angle $\theta_0 = \pi/8$ and the displacement was measured with a laser-displacement sensor. This way the damping in the rotational joint of the hammer was derived which is assumed to be equal for all joints. Figure 4-1 shows the measurement of a pendulum test for the hammer. It can be noticed from this measurement that the damping appears as velocity independent damping. This kind of damping has equal magnitude for all velocities above some threshold. The measurement shows an approximately linear decay in the oscillation and an abrupt stop

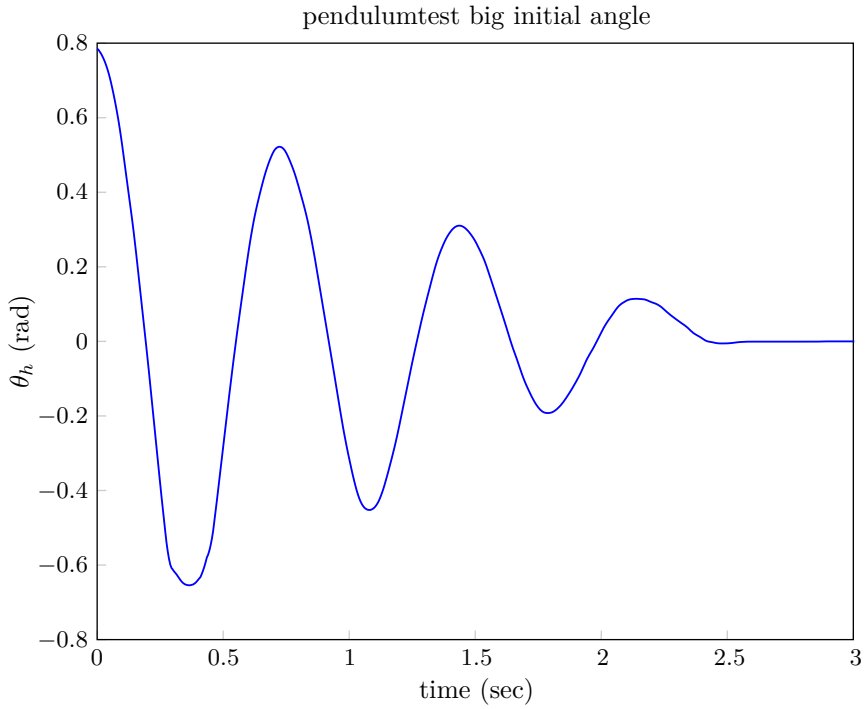

Figure 4-1: pendulumtest of hammer for $\theta_0 = \pi/8$

when the velocity becomes small. This as opposed to velocity dependent damping where an exponential decay would be present.

4-2 Rotational inertia

Equation (4-1) gives an expression for a rotational pendulum with rotational inertia I, damping d, mass m and length l. A linearization around the equilibrium $\theta = 0$ written in state space form is given as (4-2). This Equation is used to estimate the rotational inertia of the parts of the action mechanism. The mass of the different parts is determined by using a scale weight and the length l represents the vertical component of the center of mass of the parts which is calculated as shown in chapter 2-3.

$$I\ddot{\theta} + mgl\sin(\theta) = 0 \tag{4-1}$$

$$\begin{pmatrix} \Delta\dot{\theta} \\ \Delta\ddot{\theta} \end{pmatrix} = \begin{pmatrix} 0 & 1 \\ \frac{-mgl}{I} & 0 \end{pmatrix} \begin{pmatrix} \Delta\theta \\ \Delta\dot{\theta} \end{pmatrix} \tag{4-2}$$

The eigenvalues of the transition matrix in (4-2) are given as the solution of $\lambda^2 + mgl/I = 0$ which gives $\lambda = +-i\sqrt{mgl/I}$. This corresponds to an undamped eigenfrequency $\omega = \sqrt{mgl/I}$ and period of oscillation $T = 2\pi/\omega$. With the periods from the pendulum tests, the rotational inertia I is approximated. These values do not take into account the damping in the rotational joints which will be looked at in the next chapter.

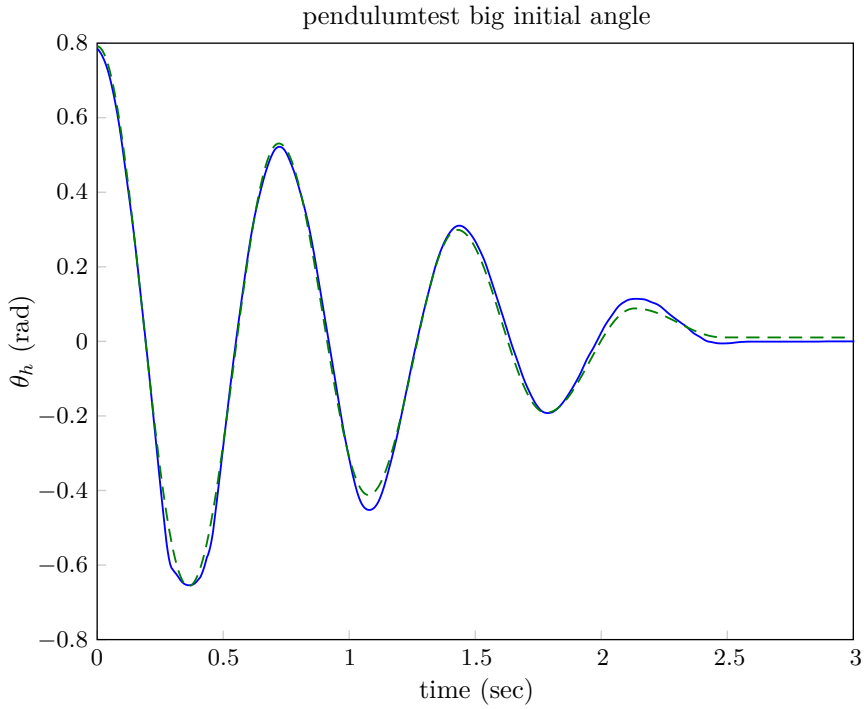

Figure 4-2: comparison of measurement and approximate hammer movement for big initial angle

mass and rotational inertia of the parts	mass (kg)	inertia (kg·m^2)
key	0.092	$2.75{\cdot}10^{-3}$
whippen	0.01	$1.69{\cdot}10^{-5}$
bridge	0.0038	$4.10{\cdot}10^{-6}$
jack	0.027	$7.78{\cdot}10^{-7}$
hammer	0.012	$1.51{\cdot}10^{-4}$

4-3 Damping in the joints and sliding friction

The damping in the felt bushed joints appears as damping that is independent of velocity as discussed in chapter 4-1. This can be modeled with a force equation (3-25). But now instead of a sliding velocity we have the angular velocity of the joint $\dot{\theta}$. This gives a damping with equal magnitude for all velocities above a threshold $\dot{\theta}_c$ which is determined experimentally.

$$I\ddot{\theta} + f_{jd}(\dot{\theta}) + mgl\sin(\theta) = 0 \tag{4-3}$$

(4-1) is augmented with this damping force to form (4-3) as the equation for a damped pendulum. This equation is implemented in a simulation and the parameter $\dot{\theta}_c$ is tuned to match the measurements as shown in figure 4-3 for a small initial angle $\theta = \pi/8$ and in figure 4-2 for a relative big initial angle $\theta = \pi/4$.

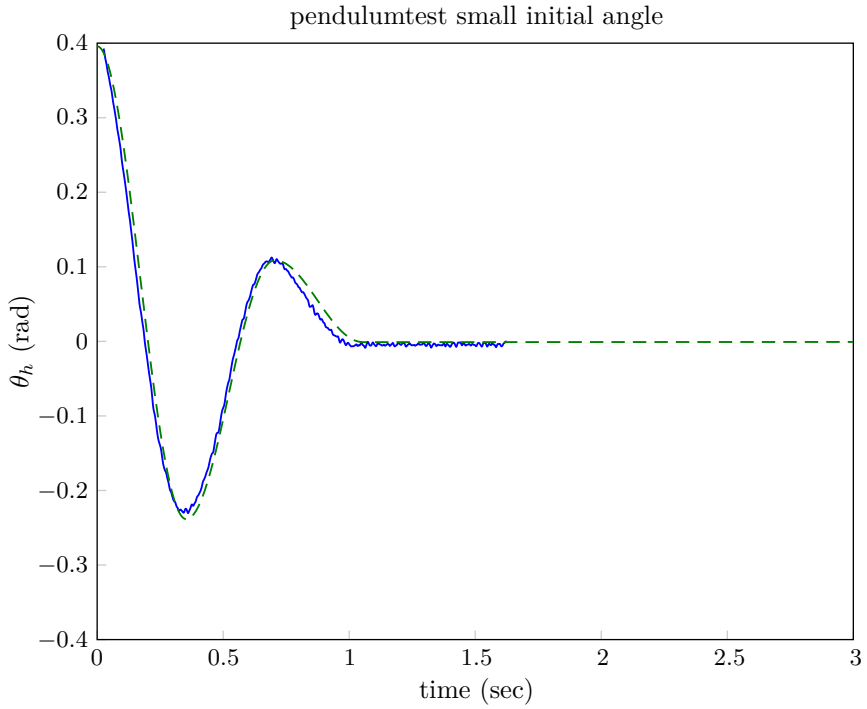

Figure 4-3: comparison of measurement and approximate hammer movement for small initial angle

damping in joints	
damping coefficient d	0.00053
velocity treshold $\dot{\theta}_c$	0.1 rad/s

The sliding friction between contacts as discussed in chapter 3-5 is first implemented in the dynamical equations and then tuned to match the measurement. However, it turned out that the effect of the friction between capstan-whippen and jack-hammer knuckle is not noticeable for medium and hard and very hard keystrokes. Only for soft key strokes the effect of the friction appears to be significant. The friction between hammer and catch is however significant for high velocities also, as will be shown in chapter 5.

4-4 Hammer-string dynamics

The force equation for the dynamics of the hammer head given in chapter 3 is tuned by fixing the string height and tuning the parameters so that the hammer trajectory for different keystrokes matches the measurements. That is, the contact time between hammer and string must be ranging from 1.5 ms to 4 ms for hard to soft keystrokes and the velocity at which the hammer bounces back must match the measurements.The magnitude of the force ranges from about 5 N to 70 N, this corresponds roughly to values given in [33]. The resulting interaction forces are shown in figure 4-5 for different intensities of key strokes. The parameter values for the hammer-string force are given in the table below. The value for the exponent p corresponds to the value used in [16], however the stiffness coefficient k was taken much lower in [16], in the order of 10^4. In [33] the value for k is taken in the order of 10^{10}. A possibility for the discrepancy between the used values and values given by others can maybe be explained by the approach with the fixed string hight. This approach for tuning the parameters does not take displacement of the string due to hammer impact into account. It can however be argued that this has just little influence on the contact time and magnitude of the interaction force.

Matched quantities	min	max
Hammer string contact time	1.5ms (ff)	4ms (pp)
Peak force hammer-string	5 N	70 N

Parameters for equation (3-26)	
Exponent p	5
Stiffness k	$0.75 \times 10^{14}\ N/m^p$

4-5 String parameters

The parameters E, I, T, μ for the wave equation are taken from [8] and E is adjusted a little to match the first harmonic frequency of the simulation and a measured signal. In [8] no damping is included in the string model and no other references were found for numerical values of the damping parameters. Hereby it is chosen to tune the damping parameters $d1$ and $d2$ so that the simulated bridge force signal matches the decay of a measured sound signal in time and frequency domain as discussed in chapter 2-6. For this, the force signals in figure 4-4 are used as an input for the string model at 1/8 of the length of the string which corresponds to a realistic impact position for the hammer.

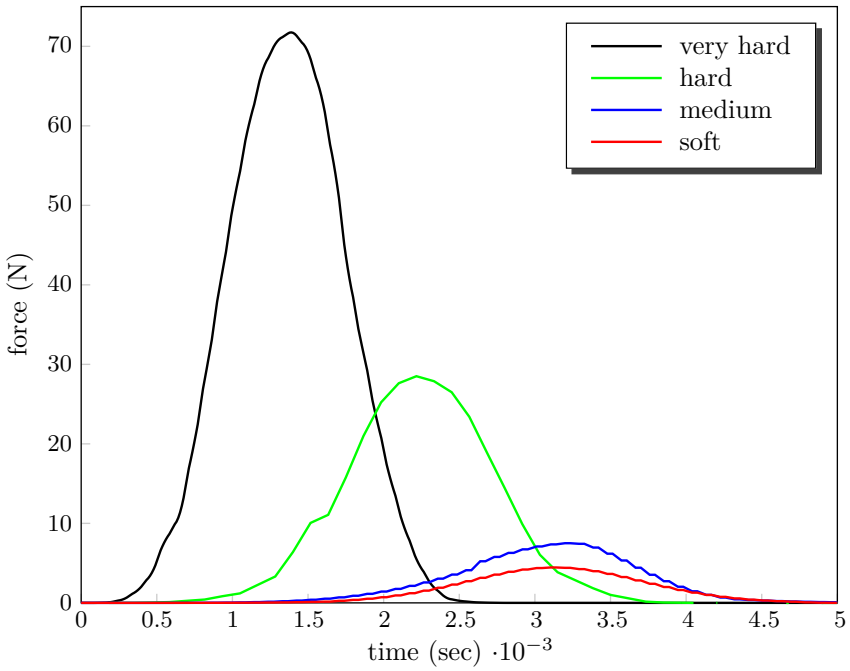

Figure 4-4: hammer - string interaction forces for different keystrokes, the parameters of the hammer-string coupling force equation are tuned such that the impact time for different keystrokes resembles measurements from video data

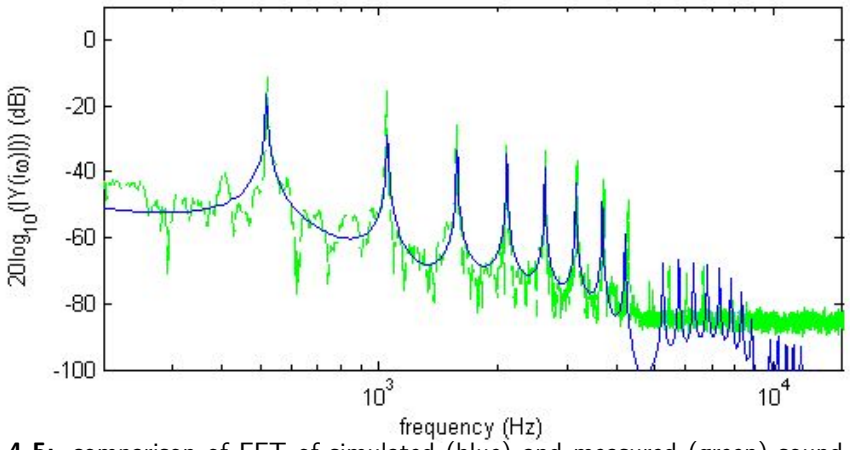

Figure 4-5: comparison of FFT of simulated (blue) and measured (green) sound for hard key stroke, the parameters of the string model are tuned such that the decay of the simulated frequencies resembles the measurement

Parameters for equation (3-27) per string	
length of the string L	0.341 (m)
impact position a	L/8 (m)
Youngs modulus E	2.2 (Mpa)
moment of inertia of cross section I	10^{-6} (kg m)
tension coefficient T	703 N
linear density coefficient μ	0.0058 kg/m
damping $d1$	0.07
damping $d2$	0.0002

Chapter 5

Simulation and validation

5-1 Structure of the simulation

The simulation of the dynamical model is built in Matlab according to the description given with the hybrid automata in chapter 3. For each motion stage, there is a set of holonomic constraints that correspond to the configuration that is combined with the dynamical equations. When a transition from one to the next motion stage takes place, the set of constraints is switched and thus the system of equations is reconfigured. This can be a change of hard constraints, or also an additional contact model. A flowchart of this simulation process is given in figure 5-1.

The transitions between the motion stages are defined as zero crossings of the transition functions g given in chapter 3. The detection of these zero crossings is done by storing the previous function value of g and when the product of the evaluation of g at a current time step with this previously stored function value is negative, then a zero crossing has occurred. This is indicated with (5-1).

$$g_t \cdot g_{t+\Delta t} \begin{cases} \leq 0 & \text{zero crossing} \\ > 0 & \text{NO zero crossing} \end{cases} \tag{5-1}$$

When a zero crossing is detected, a transition has to take place. When a hard constraint is added to the set of equations the detection of the time instance of the zero crossing has to be fairly accurate. This is caused by the fact that the contact forces are calculated on bases of the constraint values, when the detection is to late unrealistic contact forces are calculated. The time instance of the zero crossing can be made more accurate by interpolating between g_t and $g_{t+\Delta t}$. To stop the simulation and reconfigure the equations, an event-handler of the ODE solver in Matlab is used.

The model of the mechanism and the string model are simulated together and coupled trough the contact equation (3-26) to provide a realistic hammer-string interaction. To reduce the computation time of the simulation, different sample times are used for both models. The

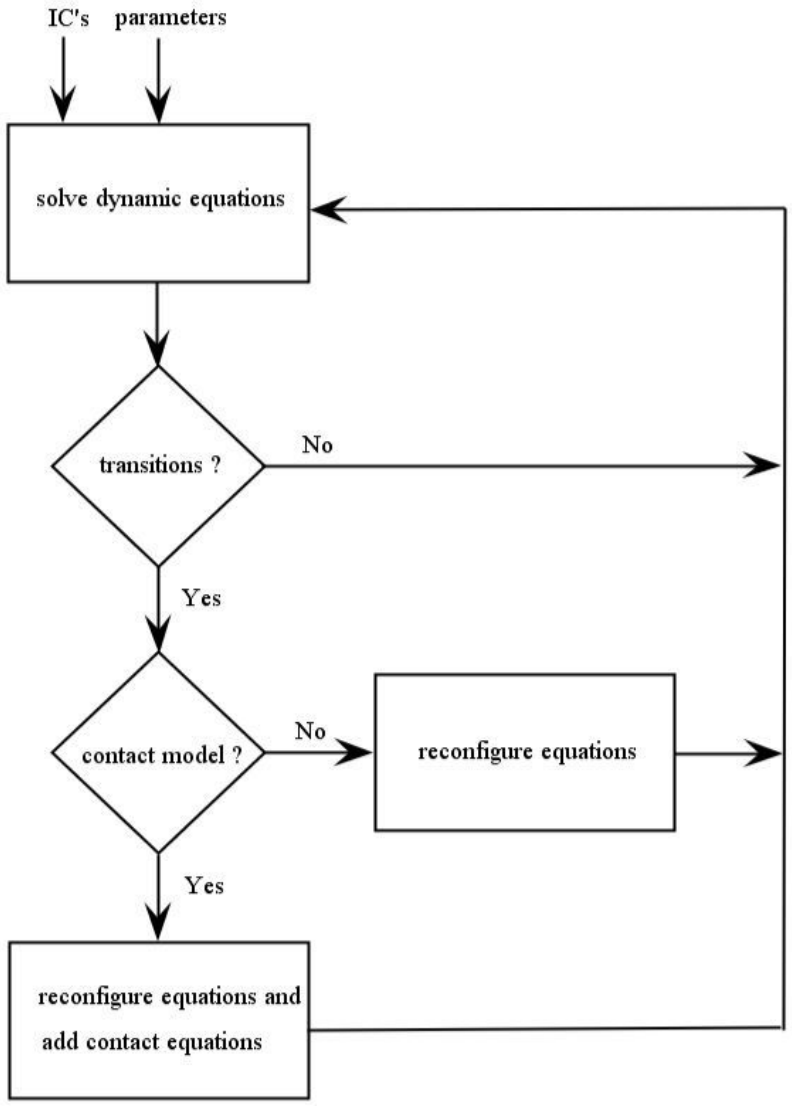

Figure 5-1: flowchart of the structure of the simulation

string model is solved with a linear solver with a fixed sample time. This sample time is selected on bases of the reasoning that to be able to compute a solution up to the nth harmonic frequency of the string, there must be at least $2n$ spatial grid points and $\Delta x = L/2n$ with L the speaking length of the string. Now with $c = \sqrt{\frac{T}{\mu}}$ as the wave propagation speed the sample time is selected so that traveling waves do not move more than one spatial step during one time step as $t_s = \Delta x/c$ *sec*. With a computed solution up to 20 kHz, which is roughly the limit for audible sound a number of 80 grid points is sufficient. This corresponds to 40 harmonic modes for a C5 string with a ground frequency of app. 523 Hz. Now the sample time is selected as $t_s = \Delta x/c = 1.1674 \cdot 10^{-5}$ *sec* for the string model. For the numerical integration of the action mechanism model a stiff ODE solver is used with a minimal sample time of 1 ms. A drawback of this method with different sample times is that the force signal that is used as an input for the string model, has to be interpolated between sample instances.

5-2 Simulation results

Figure 5-2 shows one frame of the visualization of the simulation in Matlab to make a first visual check if the configuration is valid and the angles are in a realistic range. The dynamical simulation gives the rotational angles of the five bodies and this visualization is made by plotting pictures of the five bodies that rotate with the simulated angles. The scale of the axis in figure 5-2 is in millimeters and bodies are drawn in realistic measures.

In figures 5-3, 5-4 and 5-5 the simulated rotation angles of the five bodies are given for a medium key stroke where the key is held down for little less than half a second before it is released. Figure 5-3 shows a comparison of the simulated hammer angle trajectory with a measurement that was extracted from video data. The comparison shows little discrepancies between both signals. The rotation angles of the other bodies appear to be realistic from visual inspection, also the time instances of the different events that occur during operation are compared to video data which showed a fairly good agreement.

Figure 5-6 shows simulated hammer trajectories for different intensities of keystrokes. This corresponds roughly to the range of realistic input signals to which the mechanism responds properly. The simulated signals show a realistic sensitivity to a change of intensity of the input signal which is an important property of the action mechanism as it determines the dynamic range of tones that can be produced. For the very hard and hard keystroke, the sliding friction between the bodies that is implemented in the dynamical model as explained in chapter 3, is not significant. For the medium and soft keystroke, the bodies move at lower velocities and the sliding friction appears to be more present. The friction coefficients were tuned so that simulation and measurement also match for the medium and soft keystroke.

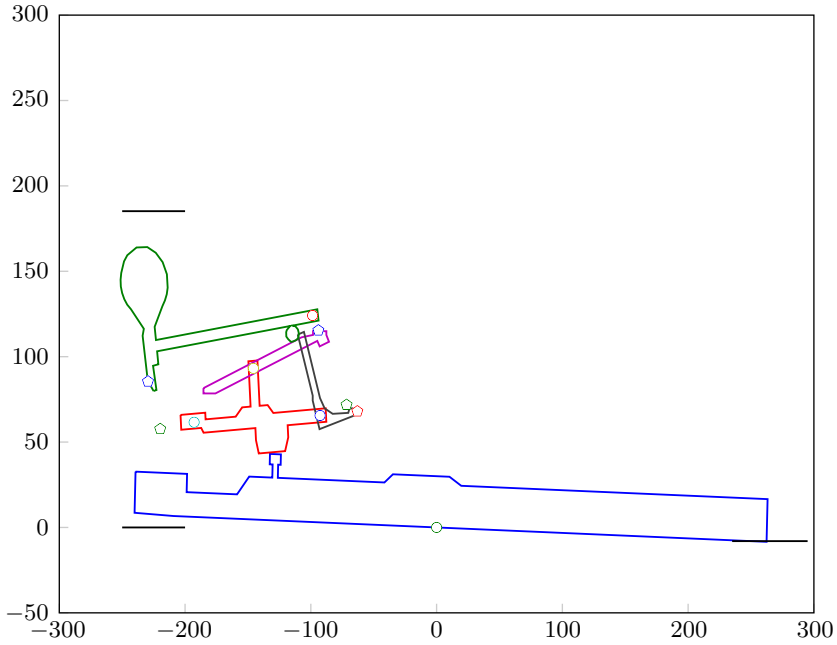

Figure 5-2: visualization of the simulation in Matlab

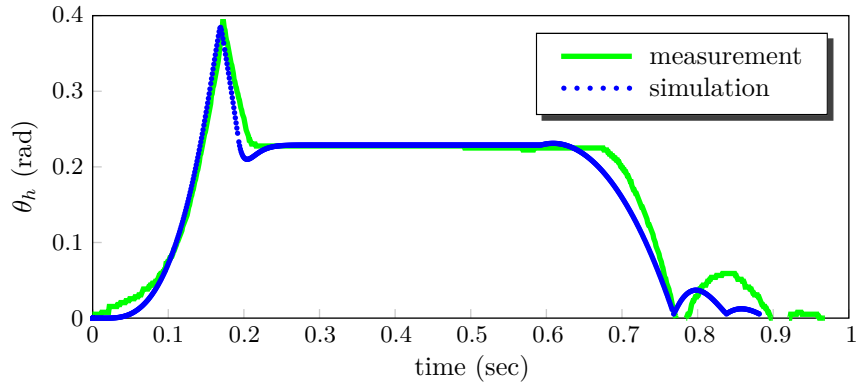

Figure 5-3: simulated hammer trajectory compared to measurement for pressed key stroke where the key is released afted about 0.5 sec

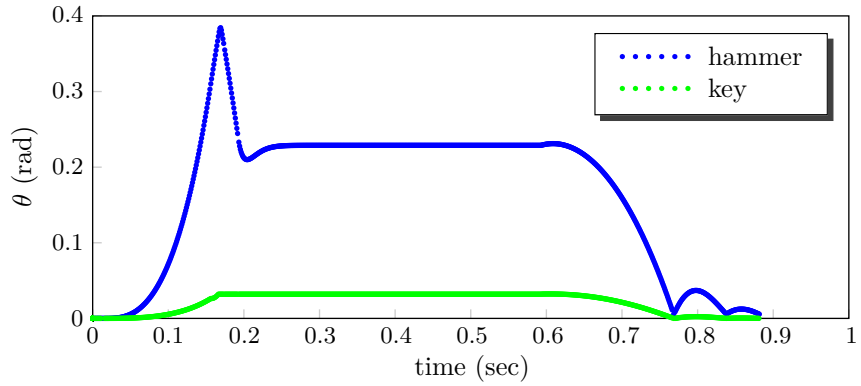

Figure 5-4: simulated hammer and key trajectory for medium keystroke

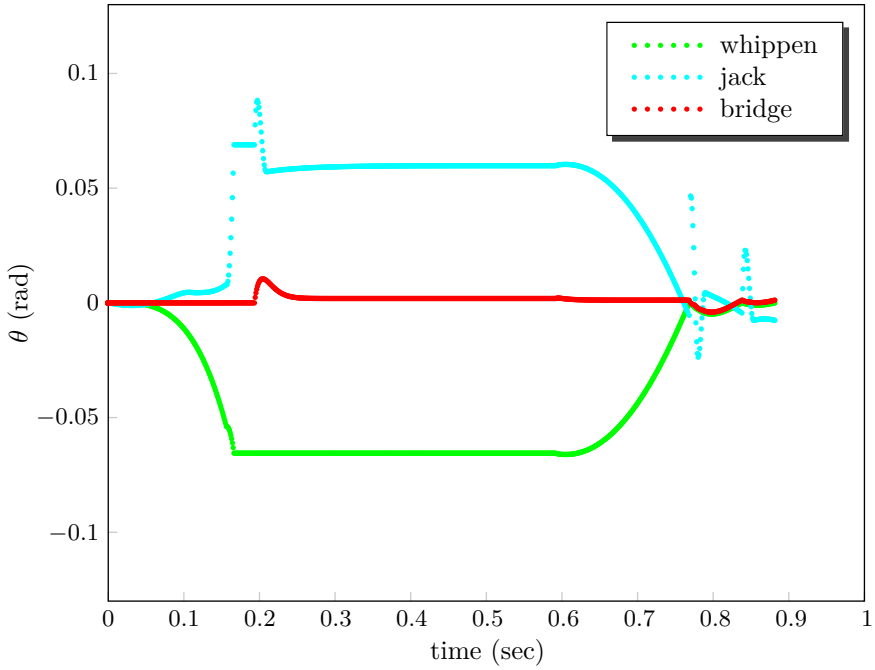

Figure 5-5: simulated whippen, jack and bridge trajectory for medium keystroke

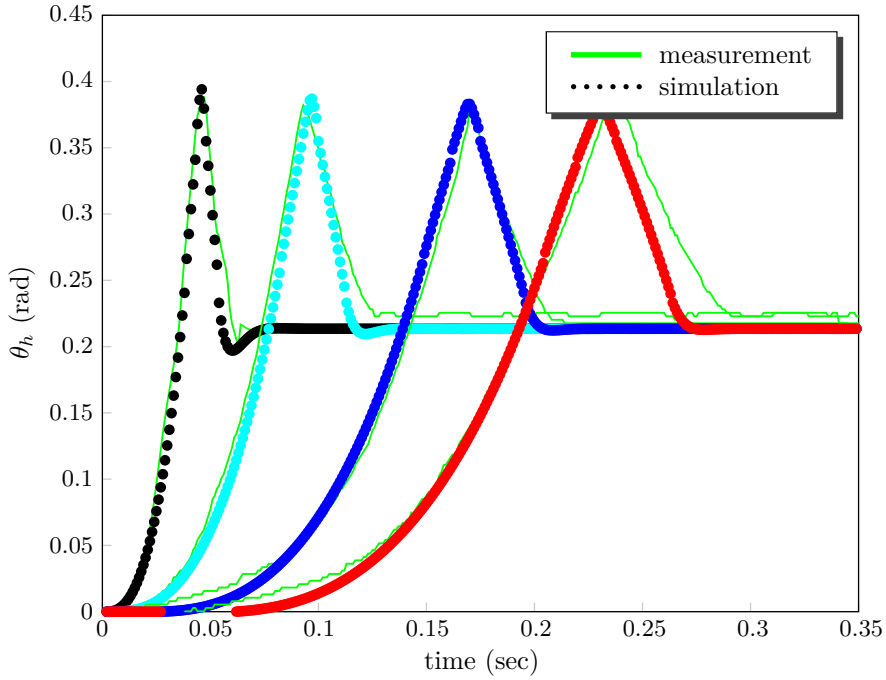

Figure 5-6: simulated hammer trajectories for different keystrokes compared to measurements

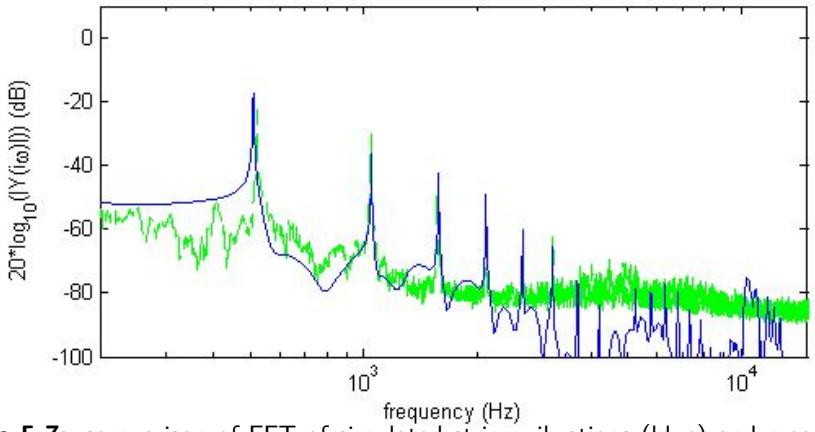

Figure 5-7: comparison of FFT of simulated string vibrations (blue) and measurement (green) for soft key stroke

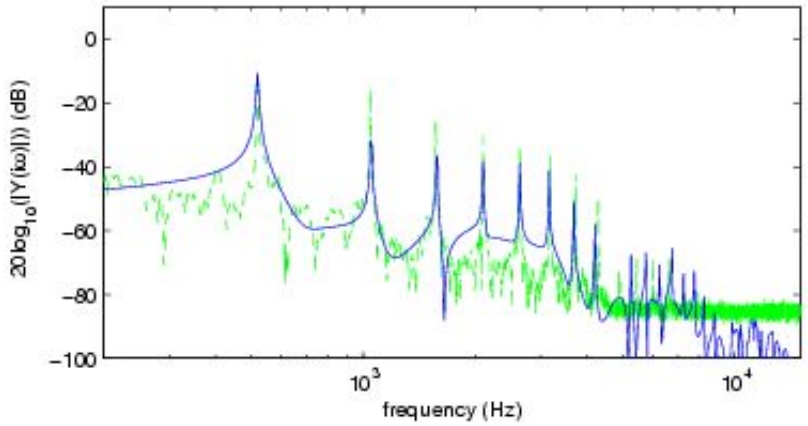

Figure 5-8: comparison of FFT of simulated string vibrations (blue) and measurement (green) for hard key stroke

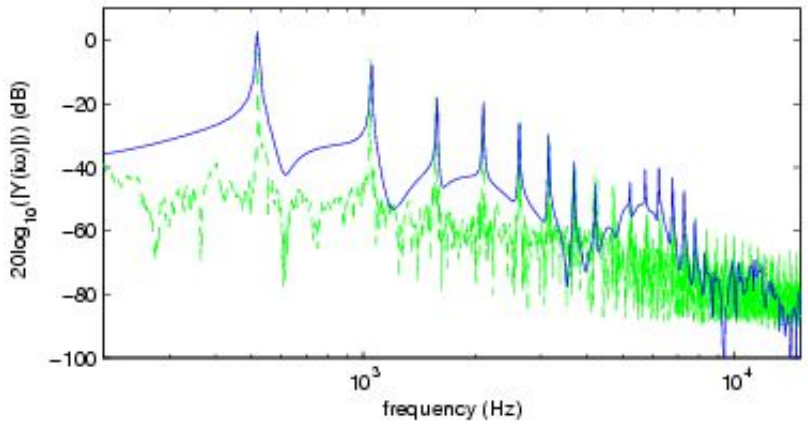

Figure 5-9: comparison of FFT of simulated string vibrations (blue) and measurement (green) for very hard key stroke

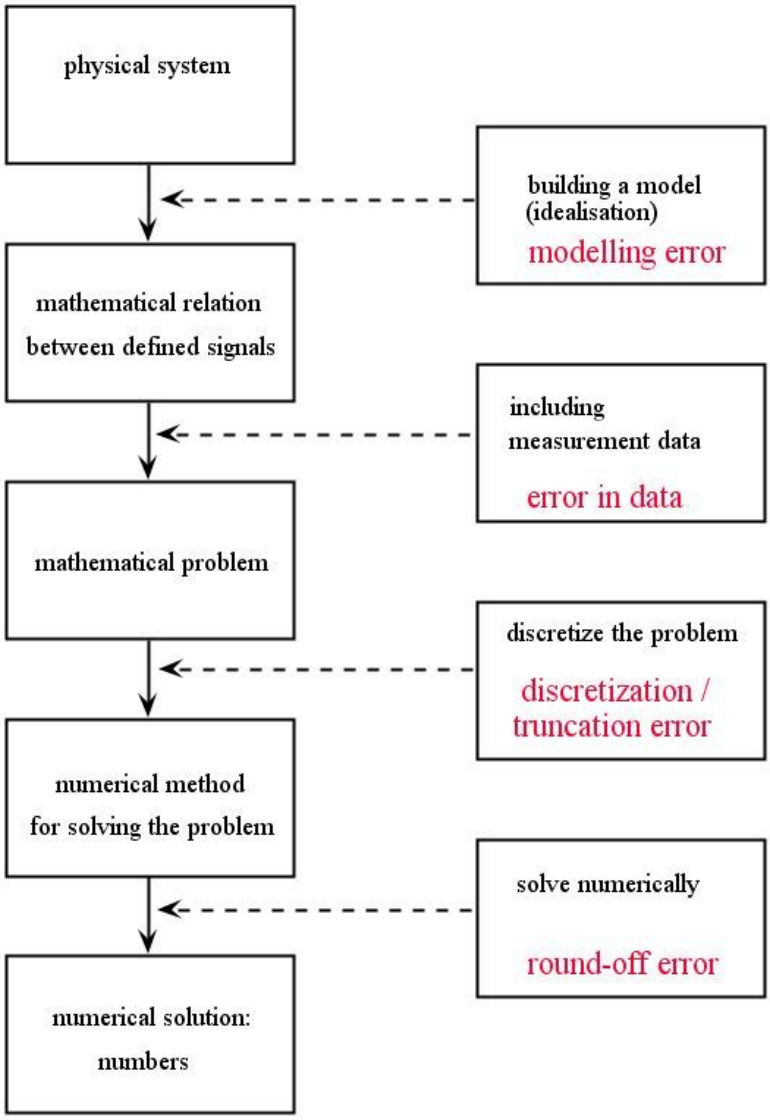

Figure 5-10: overview of errors made in the simulation (after C. Vuik and D.J.P. Lahaye [34])

5-3 Accuracy of the simulation

Figure 5-10 shows a schematics with the different sources for errors that can be present in the dynamical simulation. The following text will treat these sources separately in an attempt to get an indication of the overall accuracy of the simulation.

modeling error

As few as possible concessions are made on the accuracy of the model for the action mechanism. It is chosen to take rotational angles as degrees of freedom for the bodies of the model and the sliding contact that occurs between the parts is modeled with sliding motion between separate bodies. Nevertheless, the contacts between the bodies are not very accurately modeled. All contacts are represented with a normal vector between a point on one body and a line on the other body. This can be modeled more accurate by taking in to account the

geometric shape of the real contact surfaces. However, to be able to validate a model with such features, more accurate measurements are needed. For the string model more rigorous simplifications are made. The 1D wave equation given in chapter 3 only represents the real phenomenon to some extend. Only transverse vibrations are modeled, which means that vibrations in longitudinal direction are neglected. Also nonlinear effects that occur in real life are not modeled, the string model has fixed boundary conditions, while the boundaries of a real string vibrate because motion is transferred between strings and soundboard. In ref [26] these effects are said to be essential to mimic the sound of a real piano.

error in data

Several measurements are used to estimate model parameters and to validate the model for the mechanism and the string model. The measurements for the pendulum test from which the rotational inertia and joint friction coefficients are estimated is done with an optical laser displacement sensor with an accuracy of 0.2% for a range of 5mm, this corresponds to $10\mu m$ for the full range of the sensor. For this measurement the sensor is placed at 1mm from the joint location and the measured linear displacement x up to 2mm is used to calculate the approximate rotation angle as $\theta = arctan(x/10^{-3})$ this gives an inaccuracy within 0.2% . The different measurement signals from the piezoelectric sensor are used as input signals for the model, however these measurements are fairly inaccurate. The calibration of the sensor showed a bias error that is caused by the hysteresis effect of the sensor which is a known issue for piezoelectric material. This bias error is expected to stay within 10% of the measurement range. The measurements that were extracted from the video data also show a little deviation which is probably caused by very little variation of the lighting. A known issue for data from high speed video footage is that the lens of the camera is not properly calibrated and this can result in distortion. To prevent this, the lab setup was placed as close as possible to the camera and with the surface of the moving parts perpendicular to the lens. It is assumed that the only source of inaccuracy in the video data is the variation of the light. The measurements show a deviation maximal 5% in a stationary part of the video.

round off error

With the numerical computation, numbers of finite length are used. In Matlab a double floating point precision is the standard precision for single numbers, this is very accurate but due to the many multiplications and divisions on rounded off numbers many small errors may add up rapidly. For the ODEnnxx solvers in Matlab the digits nn indicate the orders of the solutions that are compared to calculate an absolute error. For this error a tolerance is specified as 10^{-6}. A second specification to control the round off error in the solution of the ODE solver in Matlab is the relative error tolerance. This regulates the size of the error relative to each component of the solution. This values is chosen as 0.1%.

The biggest known source of error apart from the modeling error is thus the inaccuracy of the measurements. The force measurement from which the recorded signals are used as an input for the simulation and the data that is extracted from high speed video images that is used to validate the simulation. Together, an inaccuracy of 10% seems realistic. Figure 5-11 shows the simulated hammer angle compared with a measurement with 10% deviation.

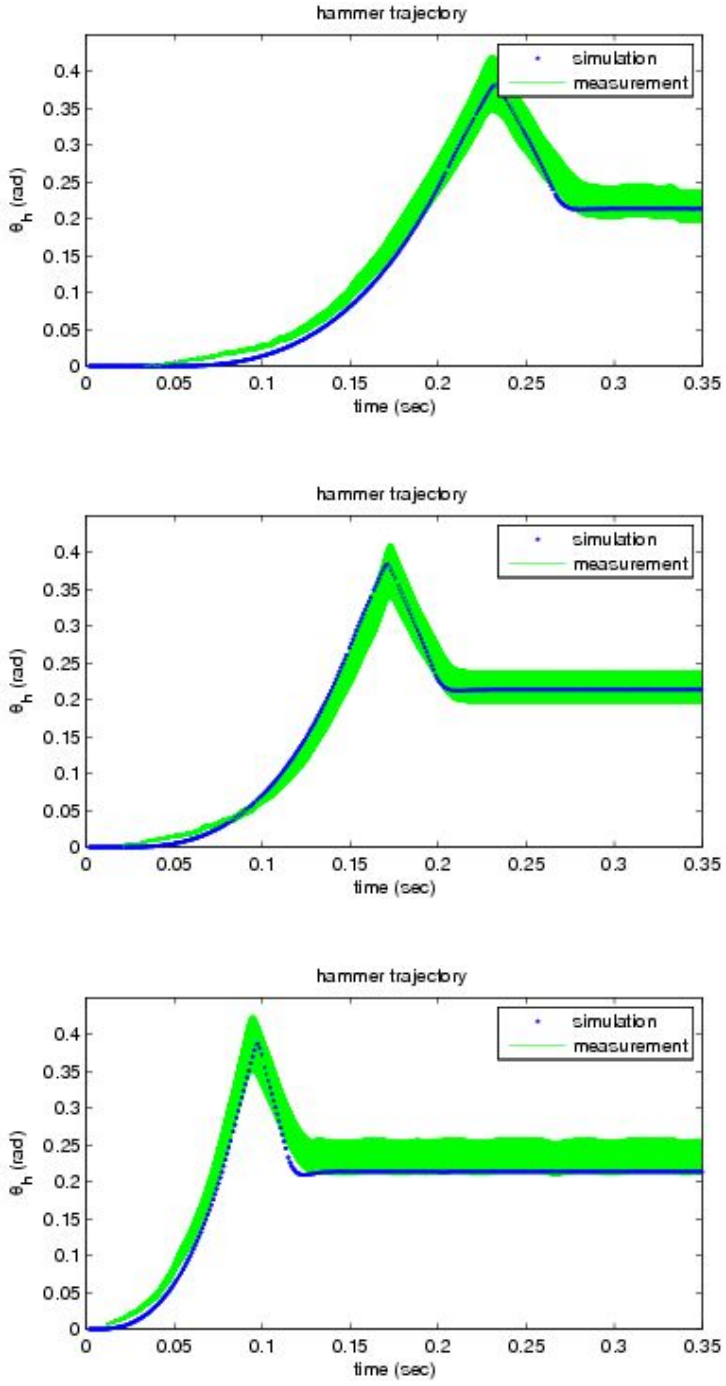

Figure 5-11: comparison of measurement +-10% and simulated hammer trajectory for soft, medium and hard keystroke

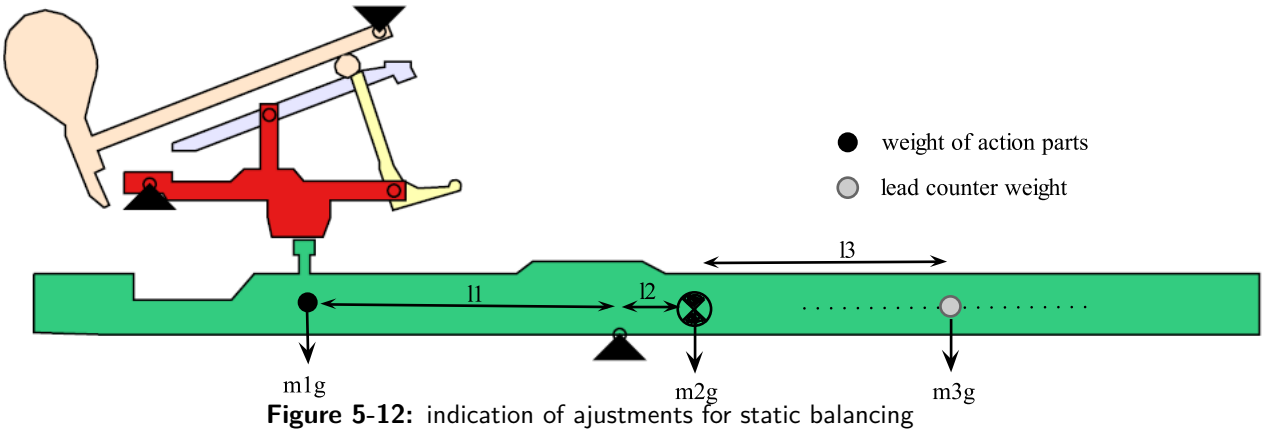

Figure 5-12: indication of ajustments for static balancing

5-4 Application to a practical problem

In chapter 2 it is already mentioned that when most grand pianos are newly built, the keyboard is statically balanced in an attempt to create an even feel over the keyboard. This is done by placing small lead rolls inside the wooden keys to compensate for the weight of the other parts of the mechanism. Also sometimes little metal rotational springs are attached to the joint of the whippen to create a similar effect. This balancing is also done by piano technicians when they replace parts of the mechanism or completely rebuild an instrument. Figure 5-12 schematically shows what is done with static balancing. When for aexample hammer heads are replaced, m_1 will change and to compensate this a lead with mass m_3 can be placed on the dotted line so that the center of gravity of the key moves as $l_2 = (m_2 l_2 + m_3 l_3)/(m_2 + m_3)$.

As from a statical point of view this balancing method seems sufficient to create an even feel, it is not from a dynamical point of view because the haptic feel that a pianist experiences is also partly influenced by the rotational inertia of the parts, and the hammer in particular. It is known that the contribution of the rotational inertia to the haptic feel is quadratically proportional to the transmission ratio of the mechanism. This indicates that this can be influenced by regulation settings that change the transmission ratio.

Figure 5-13 shows the effect of increasing the hammer mass on the hammer-string interaction force. For a heavier hammer, the contact time is little longer but the force is approximately equal in magnitude. In figure 5-14 the FFT of the simulated string vibrations shows that the simulation with increased hammer mass shows little more excited high frequencies. Figure 5-15 shows the effect on the hammer trajectory. When the hammer mass is increased, the hammer velocity will be lower compared to the lower hammer mass with equal key input force. Hence, this influences the mechanical admittance v_h/F_k which is assumed to be a measure for the haptic feel that is experienced by a pianist. With this assumption it can be said that when this ratio is decreased, the feeling of control decreases.

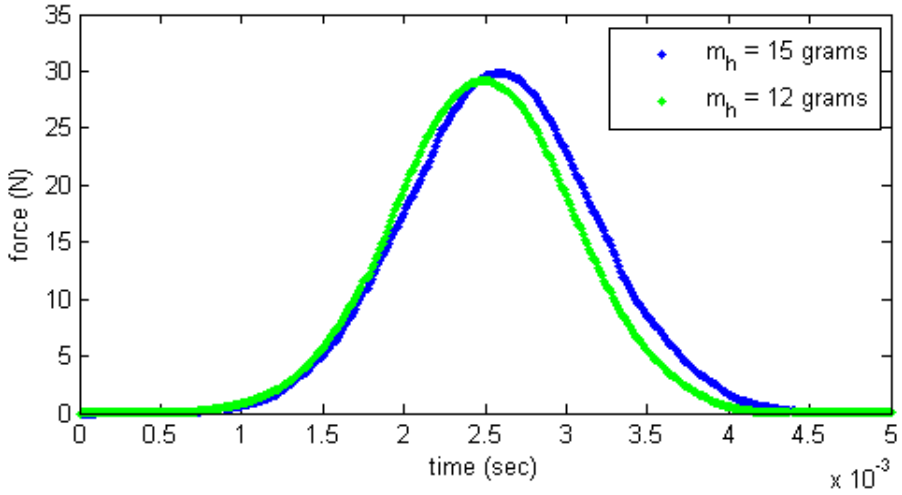

Figure 5-13: hammer - string force for hard keystroke for increased hammer mass (blue) and original (green)

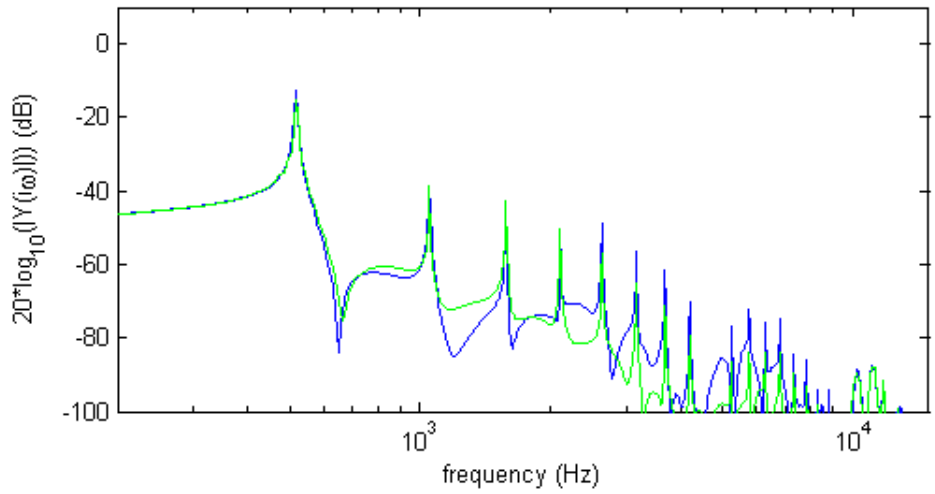

Figure 5-14: FFT of string vibrations for hard keystroke for increased hammer mass (blue) and original (green), this shows that with a heavier hammer head the contribution of higher harmonic frequencies is increased

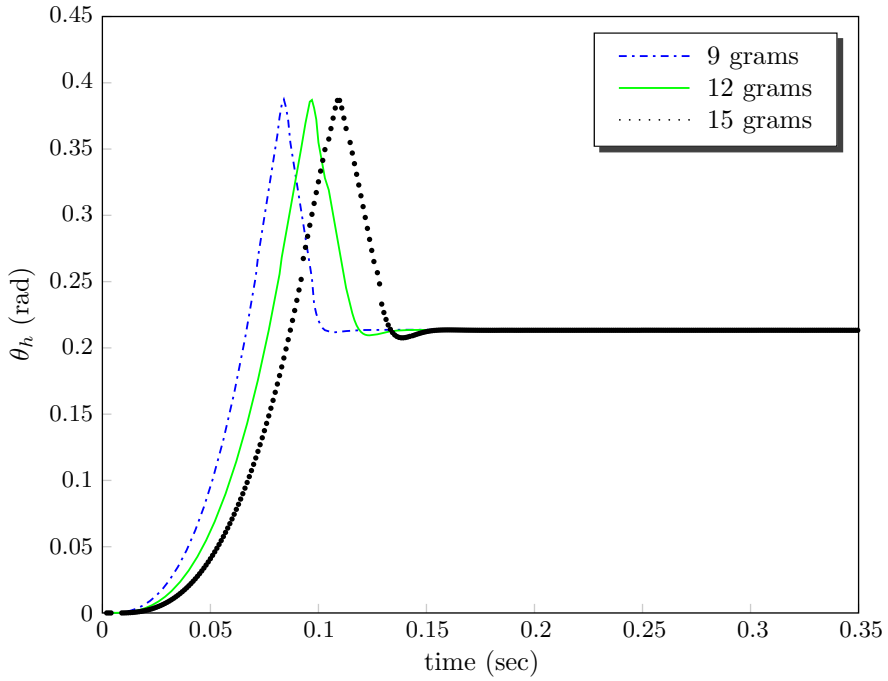

Figure 5-15: hammer angle trajectories for hard keystroke for reduced hammer mass (blue), increased hammer mass (black) and original (green), this picture shows that for increasing the mass of the hammer head the hammer velocity decreases with the same keystroke as input

Chapter 6

Discussion

In this chapter, some last remarks will be given on the developed simulation. The results will be viewed on performance of the model in terms of accuracy, usability and possible improvements. Also some interesting points for further investigation are pointed out.

The main result of the project is the developed multi body dynamical model of the grand piano action mechanism. The comparison of the simulation to the measurements that were extracted from high speed video images show an agreement within 90% to 100% for the hammer trajectory for a particular key stroke. That is when an inaccuracy of 10% is considered for the measurement signals. The discrepancy between measurement and simulation can also be sought in the concessions that are made in the development of the model. As discussed in paragraph 5-3, the contacts that are modeled with points on lines in stead of realistic geometric shapes, and also assumptions that are made for derivation of the rotational inertia for the bodies can be a source of error. This can be seen by the sensitivity to changing the hammer mass shown in paragraph 5-4. The response to different input signals is however fairly accurate, as opposed to the results presented by others there is no need to re-tune the model parameters for different input signals. The model has a physical informed structure where the five main parts of the mechanism are represented with rigid bodies with rotational joints. Because of this model structure, the geometrical and other physical properties of the bodies can be changed fairly easy or even brought out explicitly as adjustable parameters. The most used regulation properties are already implemented as adjustable parameters. Another feature of the chosen model structure is that with adjustments of the geometric shapes and contact equations, possibly also other multi body structures or mechanisms can be simulated without to much effort. The developed string model can not measure up to state of the art models where transverse and longitudinal vibration models are merged and nonlinear effects are taken in to account. However, with the coupled simulation of the action mechanism model and the linear string model for transverse vibrations at least the frequency spectrum of the sound is simulated fairly accurate for the lower frequencies. The comparison of the frequency spectrum of the simulated vibrations with the sound measurements for different intensity of keystrokes show the characteristic effects of changing the intensity. Also when the signal is played as an audio signal, the sound of a piano can be recognized. Possible improvements

on the string model are the inclusion of longitudinal vibrations, nonlinear effects like varying coefficients and flexible boundary conditions. Moreover, to improve the accuracy of interaction between both models, also a flexible body for the hammer shaft of the action mechanism can be included. Research at the Waterloo university showed that scuffing motion between hammer and string during contact can influence the harmonic frequencies that are excited in the string motion. Where this scuffing motion is due to the flexibility in the hammer shaft. Another interesting point for further investigation is the haptic touch of the mechanism. It was attempted in paragraph 5-4 to show a practical application of the simulation, by using it to show how adjustments to regulation settings can be used for dynamical balancing of the key board. To make a more thorough analysis of such application, it can be of use to first investigate systematically how changes of different properties are experienced by a pianist when playing the instrument.

The achievements of this project in a few statements:

- A dynamical simulation of the action mechanism in a grand piano was developed. The motion of the five main parts of the mechanism can be simulated for different intensities of keystrokes. For this simulation the most often used regulation settings are implemented as parameters that can be adjusted.
- A dynamical simulation of a string in a grand piano was developed and this simulation was coupled with the simulation of the action mechanism to form a parallel simulation. With this simulation the effect on the produced tone can be investigated, this can be of use when parts are replaced.
- The simulation was analyzed in terms of accuracy and usability. The simulation of both the mechanism and string show a good agreement with measurements. A possible application to a practical problem is given.
- Possible improvements of the simulation were pointed out. The mechanism model can be extended with a flexible body for the hammer shaft and more realistic contact shapes.
- Interesting subjects for further study were pointed out. The haptic touch of the mechanism can be an interesting subject for further investigation. When it is systematically investigated what factors determine the feeling of control of a pianist, a simulation can make predictions about the effect of changing settings or parts on the touch.

Appendix A

configuration of the bodies

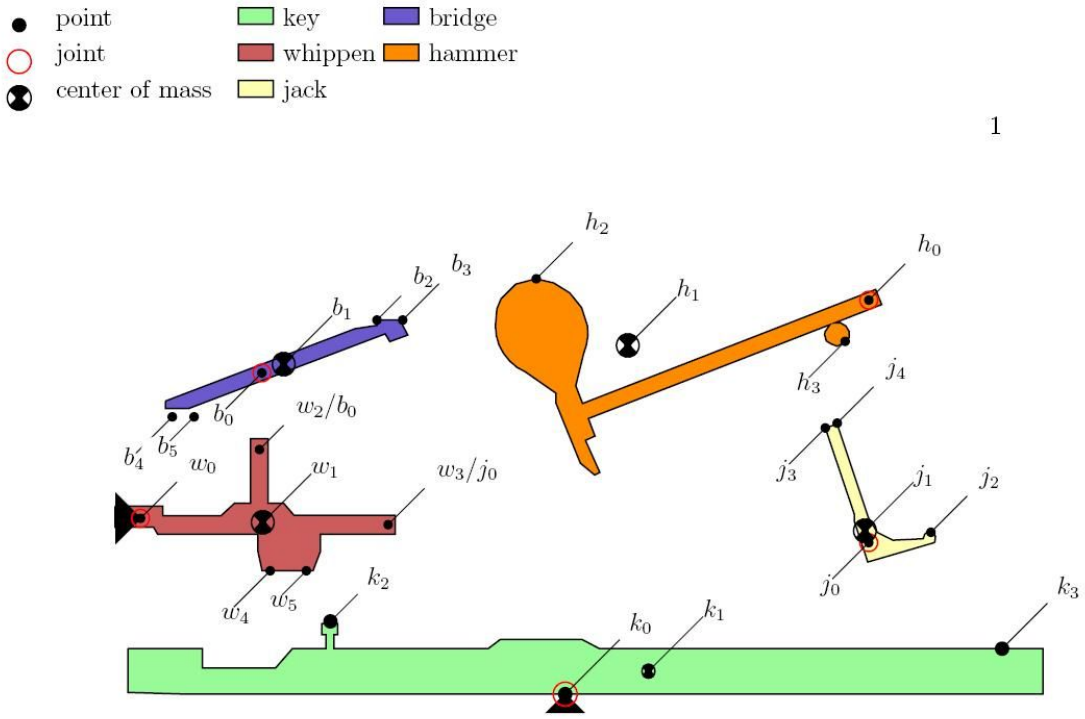

Figure A-1: bodies with locations and names of points on joint locations, center of mass and contact points

Appendix B

regulation procedure

1. Capstan screw

First the hammer height is adjusted. The hammer height is the distance between the string and the hammer when the hammer is in its rest position, this can be adjusted with the capstan. Usual distances vary of 44 up to 48 mm

2. Bridge/repetition lever regulating screw

With this regulating screw the distance between the jack and knuckle is adjusted. This distance must be as small possible (approximately 0.2 mm) keeping the control concerning the hammer optimal. In contrast with this, the jack and knuckle can make no contact in rest because the jack must reverse under the knuckle after a key stroke.

3. Jack regulator screw

With the jack regulator screw the inside surface of the jack (at the side of the hammer) is aligned with the inside of the wooden core of the knuckle.

4. Set off regulating button

The set off is the smallest distance between the hammer and string where the jack is still in contact with the knuckle. This distance is established with the set off regulating button, as the whippen travels up the jack toe will reach a standstill as a result of which the jack will turn away from under the knuckle. (Schimmel gives the following values for the set off: 2 up to 3 mm in the bass, 1.5 up to 2 mm in the mid-register, and 1 up to 1.5 mm in the diskant. S& S uses a set off value of 1 mm, and in the bass a value which corresponds to half the string width.

5. Drop screw

The hammer drop is distance which the hammer falls back after the set off. The Drop screw must be regulated such that the repetition lever stops before the jack will turn away from under the knuckle. Because of this, the knuckle will fall back on the repetition lever after a key stroke, also if the key remains pressed. Commonly used hammer drop distances are 2 mm for all registers.

6. key travel distance and after-touch

The key-travel distance is the distance the key travels (in vertical direction at the side where the key is pressed) from rest until the point where it is stopped by the front pinch punch. The key-travel distance varies from about 9 mm up to 10.5 mm. The after-touch is the last bit of this distance where the jack is already turned away from under the knuckle. A small after-touch is a condition for fast tone repetition. The ratio between key travel distance and after-touch is also a measure for the time that the pianist has control over the hammer velocity.

Bibliography

1. P.R. Dijksterhuis (1965), De piano, Nederlandse Akoest. Genootschp,Vol.7, pp.50-65.
2. A. Askenfelt and E. V. Jansson (1990), "From touch to string vibrations. I: Timing in the grand piano action," J. Acoust. Soc. Am. 88, 52-62
3. B. Gillespie (1994), Virtual piano action: Design and implementation, Centre for Computer Research Musical Acoustics ,Stanford University
4. B. Gillespie (1996), Haptic Display of Systems with Changing Kinematic Constraints: The Virtual Piano Action. PhD thesis, Stanford University , http://www-personal.umich.edu/ brentg/
5. Martin Hirschkorn (2004), MSc thesis Dynamic model of a piano action mechanism University of Waterloo, department of Systems Design Engineering
6. M. Hirschkorn, J. McPhee, and S. Birkett (2006), Dynamic modelling and experimental testing of piano action mechanism, ASME J. Comput. NonlinearDyn. 1, 4755-2006.
7. Adel Izadbaksh, J. McPhee, and S. Birkett (2008), Dynamic modelling and experimental testing of piano action mechanism with a flexible hammer shank, ASME J. Comput. NonlinearDyn. 1, 4755-2006.
8. Chandrika P. Vyasarayani, Stephen Birkett(2009), Modeling the dynamics of a compliant piano action mechanism impacting an elastic stiff string , Acoustical Society of America. Pages: 40344042
9. H. Suzuki and I. Nakamura (1990), Acoustics of pianos, Appl. Acoustics, 30, 147-205
10. E Hayashi, M Yamane & H Mori. Behavior of piano-action in a grand piano. I. Analysis of the motion of the hammer prior to string contact. JASA 105(1999):3534-3544.
11. Goebl, Bresin and Galembo (2005), Touch and temporal behaviour of grand piano actions
12. D.Colomaniciu and P.Meer, "Mean shift analysis and applications", IEEE international conference on computer vision (vol. 2, p.1197), 1999
13. Learning OpenCv, Gary Bradski & Adrian Kaebler

14. D. Russell and T. Rossing (1998)Testing the Nonlinearity of Piano Hammers Using Residual Shock Spectra Physics Department, Northern Illinois University

15. A. Askenfelt and E. V. Jansson, "From touch to string vibrations. III: String motion and spectra," J. Acoust. Soc. Am. 93 2181-2196 (1993)

16. D. E. Hall (1992), "Piano string excitation VI: Nonlinear modeling," J. Acoust. Soc. Am. 92, 95-105

17. N.H. Fletcher and T.D. Rossing. The Physics of Musical Instruments. Springer- Verlag. reviewed edition, 1991.

18. Gareth Lay, Musimathics volume 2 the mathematical foundations of music.

19. R.Q. van der Linde, A.L. Schwab, Lecture notes Multibody dynamics B, TUDelft

20. Daniel J. Rixen, Engineering Dynamics Lecture Notes Draft, V 3.0, TUDelft

21. Numerical methods in scientific computing, J. van Kan, A.Segal, F.Vermolen

22. Hermann von Helmholtz: English translation of the fourth edition in 1885 by A. J. Ellis: On the Sensations of Tone as a Physiological Basis for the Theory of Music, reprinted (paperback) by Dover Publications Inc., New York 1954. (In particular chapter IV: p49-65 and chap V.3 p74-80 with appendices III, IV, and V containing the mathematical explanation of the text.)

23. Harry Koopman onderhoud en het afregelen van het vleugelmechaniek, Piano Bulletin 1994 EPTA NLD

24. Hong Cheng Chin (1995), Stabilization methods for simulations of constrained multi-body dynamics, PhD thesis dept. mathematics, University of British Colombia, Canada

25. Birkett (2003), Static and dynamic balancing of a piano key, University of Waterloo, department of Systems Design Engineering

26. Balázs Bank (2006),Physics-based Sound Synthesis of String Instruments, PhD thesis, Budapest University of Technology and Economics, Department of Measurement and Information Systems

27. Javier Garcia de Jalon and Eduardo Bayo, Kinematic and dynamic symulation of multi-body systems

28. Michael Bradley Cline (2002), Rigid Body Simulation with Contact and Constraints,The University of British Columbia

29. R. Brent Gillespie, J. Edward Colgate, A survey of multibody dynamics for virtual environments, Department of Mechanical Engineering, Northwestern University

30. Fan-Chung Tseng, Zheng-Dong Ma, Gregory M.Hulbert, Efficient numerical solutions of constrained multi body dynamic systems, University of michigan.

31. Simulating Mechanical Systems in Simulink with SimMechanics, Giles D. Wood, Dallas C. Kennedy, The MathWorks

32. Andy Ruina and Rudra Pratap 1992-2009, Introduction to Statics and Dynamics

33. Julien Bensa,Olivier Gipouloux and Richard Kronland-Martinet, Parameter fitting for piano sound synthesis by physical modeling

34. C. Vuik and D.J.P. Lahaye, Scientific Computing 2010

35. B. De Schutter, M.Heemels, Modeling and control of hybrid systems 2009

36. T.J.J van den Boom, B. De Schutter, Optimization for systems and control 2007

List of symbols

θ_x	angle for body x
$\boldsymbol{u}_k(\theta_x)$	position coordinates with respect to stationary frame
$\boldsymbol{\nu}_k(\theta_x)$	position coordinates with respect to the joint of the body
$\boldsymbol{\xi}_k$	rigidly constrained distances between point k and the joint on a body
$\boldsymbol{R}(\theta_x)$	rotation matrix
c_i	contact i between two bodies
ϵ_i	constraint distance for contact c_i
$\boldsymbol{q}$	vector with generalized coordinates
$T(\dot{\boldsymbol{q}}, \boldsymbol{q})$	kinetic energy
$V(\boldsymbol{q})$	potential energy
$\boldsymbol{Q}^{ncons}$	vector with non-conservative forces
$\boldsymbol{M}(\boldsymbol{q})$	mass matrix
$\boldsymbol{f}(\dot{\boldsymbol{q}}, \boldsymbol{q})$	vector with generalized forces
$\boldsymbol{D}(\boldsymbol{q})$	vector with additional holonomic constraints
$\dot{\boldsymbol{D}}$	vector with time derivative of elements of $\boldsymbol{D}$
$\boldsymbol{\Phi}(\boldsymbol{q})$	matrix with partial derivatives of $\boldsymbol{D}$
$\boldsymbol{\lambda}$	vector with Lagrange multipliers
$(\dot{\boldsymbol{q}}_n\ \boldsymbol{q}_n)$	computed numerical values for generalized coordinates
$(\tilde{\dot{\boldsymbol{q}}}_n\ \tilde{\boldsymbol{q}}_n)$	corrected numerical values that satisfy the constraints
g_i	transition function
$\dot{\delta}_i$	sliding velocity between bodies for contact i

$f_c(\dot{\delta})$	function to approximate Coulomb friction
$f_n(\epsilon, \dot{\epsilon})$	normal force between bodies that are in contact
$f_d(\epsilon, \dot{\delta})$	force for sliding friction
η	vertical coordinate for contact part of the string
x	horizontal coordinate of the string
y	vertical coordinate of the string
f_{hs}	hammer-string contact force
μ	linear density coefficient
T	linear tension coefficient
E	Youngs modulus
I	moment of inertia
$\boldsymbol{A}_i$	coefficient matrix for discretized string model